The Pennsylvania State University
The Graduate School

SAFE AUTONOMOUS FLARE AND LANDING DURING AUTOROTATION THROUGH WIND SHEAR

A Thesis in
Aerospace Engineering
by
Nicholas Grande

Submitted in Partial Fulfillment
of the Requirements
for the Degree of

Master of Science

August 2013

The thesis of Nicholas Grande was reviewed and approved* by the following:

Jacob W. Langelaan
Associate Professor of Aerospace Engineering
Thesis Advisor

Joseph F. Horn
Associate Professor of Aerospace Engineering

George A. Lesieutre
Professor of Aerospace Engineering
Head of the Department of Aerospace Engineering

*Signatures are on file in the Graduate School.

Abstract

This thesis presents a method to compute the set of steady-state autorotation conditions from which safe flare to landing through wind shear can be performed. Equations of motion of a helicopter in autorotation through wind shear are presented; these equations are used to compute an optimal trajectory to landing from candidate initial states (distance and height above the touchdown point, horizontal speed, descent rate, rotor speed) to a designated touchdown point. The effect of wind shear on these optimal trajectories and on the set of safe initial conditions is examined for two rotorcraft: the Bell OH-58A and a small electric-powered helicopter. The feasibility of using waypoint following control for autorotation landing is examined for the electric-powered helicopter.

Table of Contents

List of Figures vii

List of Tables ix

List of Symbols x

Acknowledgments xii

Chapter 1
Introduction 1
1.1 Motivation . . . 2
1.2 Stages of a Safe Autorotation . . . 3
1.3 Flare in Wind Shear . . . 5
1.4 Review of Related Work . . . 6
1.5 Contributions . . . 7
1.6 Reader's Guide . . . 7

Chapter 2
The Flare Maneuver Through a Wind Shear Profile 9
2.1 Problem Statement . . . 9
2.2 Defining the Shear Profile . . . 11
2.3 Equations of Motion . . . 13
2.3.1 Autorotation Governing Equations . . . 13
2.3.2 Wind Shear Equations of Motion . . . 15
2.3.3 Incorporating Wind Shear . . . 16
2.3.4 Height-Parameterized Equations of Motion . . . 16
2.4 Optimal Trajectory Generation for Flare in Shear . . . 18
2.5 Summary . . . 19

Chapter 3
Computing the Safe Landing Set **22**
3.1 The Safe Landing Set . . . 22
3.2 Trajectory Optimization . . . 23
3.2.1 State Cost . . . 24
3.2.2 Touchdown Cost . . . 25
3.2.3 Optimization . . . 26
3.3 Safe Set Algorithm . . . 27
3.4 Summary . . . 29

Chapter 4
Safe Landing Set Simulation Results **31**
4.1 Simulation Approach . . . 31
4.2 Visualizing the Safe Landing Set . . . 32
4.3 Various Cases for Headwinds and Tailwinds . . . 32
4.4 OH-58A Results . . . 33
4.4.1 OH-58 Vehicle Properties . . . 33
4.4.2 OH-58 Safe Landing Sets . . . 36
4.5 Hornet Mini Results . . . 40
4.5.1 Hornet Mini Vehicle Properties . . . 40
4.5.2 Hornet Mini Safe Landing Sets . . . 43
4.6 H-V Diagram . . . 45
4.7 Summary . . . 48

Chapter 5
Flight Simulation Results **51**
5.1 Description of Vehicle . . . 51
5.2 Waypoint-Generated Flare Trajectory . . . 51
5.2.1 Waypoint Height Sensitivity . . . 53
5.3 Summary . . . 56

Chapter 6
Conclusion **57**
6.1 Summary of Contributions . . . 58
6.1.1 Effect of Wind Shear on the Safe Landing Set . . . 58
6.1.2 Safe Landing Sets for the OH-58 and Hornet Mini Flying Through Wind Shear . . . 59
6.1.3 Simulation Results . . . 60
6.2 Recommendations for Future Work . . . 60
6.2.1 Landing Site Selection . . . 60

6.2.2 Robustness of Safe Set Algorithm 61
6.2.3 Hardware Implementation Using Waypoint Control 61
6.2.4 Full Trajectory Implementation on the Hornet Mini 61

Bibliography **62**

List of Figures

1.1 Autonomous helicopters. Image credits: [a]: Northrop Grumman; [b]: Boeing; [c]: Lockhead Martin. 2
1.2 Stages of autorotation: engine failure, entry, descent, and flare. . . . 4
1.3 Wind shear profile. 6

2.1 Schematic of the autorotation scenario. 10
2.2 Wind shear profiles for light, moderate, and severe wind conditions. 12
2.3 Schematic of the height-discretized flare trajectory optimization problem. The target touchdown point is at the origin, the shaded region denotes terrain [2]. 17

3.1 Sample barrier function. 24
3.2 Control Spline Initial Guess 26
3.3 Helicopters used in flare analysis. 28

4.1 Bounded region of the safe landing set for the OH-58 in zero wind. . 33
4.2 Autorotation trim states for the Bell OH-58. 34
4.3 Flare region for the OH-58. 37
4.4 Total safe landing set for the OH-58 acting in various wind conditions. 38
4.5 Safe flare regions for the OH-58 that result in at least five safe landings for each wind condition. 39
4.6 Flare trajectories for the OH-58 starting at the same initial conditions under light headwind, light tailwind, and no wind conditions. 41
4.7 Autorotation trim states for Hornet Mini. 42
4.8 Flare region for the Hornet Mini. 44
4.9 Total safe landing set for the Hornet Mini acting in various wind conditions. 45
4.10 Flare trajectories for the Hornet Mini starting at the same initial conditions under light headwind and no wind conditions. 46
4.11 H-V diagram for the OH-58 [18]. 47
4.12 H-V diagram for the OH-58 from the safe landing set. 49

5.1 Hornet simulation flare trajectory using three waypoints for entry, initiation, and touchdown. 52
5.2 Comparison of the planned Hornet flare maneuver with the simulated maneuver. (Note: the helicopter images are not drawn to scale). 54
5.3 Multiple flare trajectories for various initiation and touchdown waypoint height combinations. 55

List of Tables

2.1 Wind Shear Profile Intensity 12

4.1 Parameters of the OH-58A 35
4.2 OH-58 State and Control Limits 35
4.3 OH-58 Touchdown Conditions 35
4.4 Parameters of the Hornet Mini 42
4.5 Hornet State and Control Limits 43
4.6 Hornet Touchdown Conditions 43

5.1 Hornet Mini planned and simulated touchdown conditions (using GPS waypoint navigation). 53

List of Symbols

C	Cost Function
c_{d0}	Main Rotor Profile Drag Coefficient
C_P	Power Coefficient
C_T	Thrust Coefficient
C_w	Weight Coefficient
C_x	Horizontal Component of Thrust Coefficient
C_z	Vertical Component of Thrust Coefficient
d	Horizontal Distance from Touchdown Point
f_e	Fuselage Equivalent Flat Plate Area
f_G	Ground Effect Factor
f_I	Induced Velocity Factor
h	Height above Touchdown Point
H_R	Rotor Height
I_R	Main Rotor Polar Moment of Inertia
K_{ind}	Induced Velocity Factor
m	Helicopter Mass
P_{res}	Residual Power After Simulated Engine Failure

P_s	Available Shaft Power
R	Main Rotor Radius
u	Horizontal Velocity
$\mathbf{u}$	Control Vector
u_{20}	Wind Velocity at 20 feet
v	Induced Velocity
v_h	Hover Induced Velocity
w	Descent Rate
w_x	Horizontal Wind Velocity
w_z	Vertical Wind Velocity
x	Horizontal Position
$\mathbf{x}$	Vehicle State Vector
z_0	Surface Roughness Factor
α	Main Rotor Tip-Path-Plane Angle
γ	Cost Function Weight
η	Power Efficiency Factor
θ	Aircraft Pitch Angle
λ	Main Rotor Inflow Ratio
ρ	Air Density
σ	Main Rotor Solidity
Ω	Main Rotor Angular Speed

Acknowledgments

The work presented in this thesis was achieved through the guidance and support of many different people. I would first like to thank my parents, who have supported me in every decision I have made in my academic career. Their constant encouragement has made my path much easier to follow, and while this brief paragraph cannot truly express my gratitude, I want to thank them for the love and support they show me every day.

Secondly I would like to thank my advisor, Dr. Jack Langelaan. I had the privilege of getting to know Jack as a senior, and was fortunate enough to work under him as a graduate student. Jack is all that I could have asked for in an advisor. His ability to convey information in a way that is both clear and logical allows him to get the best out of all of his students. I am very fortunate to have spent the last two-plus years working for him, and I appreciate the opportunity.

I would also like to thank Dr. Joseph Horn and Dr. Eric Johnson for their support and guidance throughout my time as graduate student: Dr. Horn for reviewing my thesis as well as providing knowledge and insight to my research, and Dr. Johnson for his ongoing technical support regarding the Hornet Mini.

A special thanks goes out to the Original Four: Sean Marlow, Anjan Chakrabarty, Nate Depenbusch, and Jack Quindlen. Upon joining the lab, they made me feel welcome from the first day, and have made each day since a fun, albeit interesting, experience. I surely cannot forget John Bird, whose breadth of knowledge is immeasurable, but somehow found the patience to explain it all to me. And of course Kwok Cheng, the permanent resident of the lab, whose presence always made those late nights tolerable.

Finally, I owe a great deal of gratitude to the Vertical Lift Consortium for funding this project and allowing me the opportunity to contribute to the rotorcraft community.

Dedication

This thesis is dedicated to the future members of the AVIA lab. May the company you find here be as entertaining as mine was.

Chapter 1

Introduction

This thesis describes a method for determining a safe region from which an unmanned aerial vehicle (UAV) helicopter can initiate flare during autorotation under the influence of wind shear. Simulation results are provided for two separate helicopters: a mid-size utility helicopter and a small-scale autonomous helicopter. Additionally, flight simulation results of the trajectory planning algorithm for the small-scale helicopter are presented. The motivation for this research is the ever-present possibility of a power or transmission failure in a helicopter, both manned and unmanned. The resulting autorotative flight condition is exceedingly dangerous, but the UAV must be capable of executing the full trajectory, from engine failure to touchdown. The final flare maneuver is especially challenging due to the helicopter's close proximity to the ground and the short time period over which the maneuver occurs.

Additional motivation comes from the necessity to accurately model the influence of wind on the flight of the helicopter. Much of the research done in this area assumes zero wind conditions throughout the flight. Realistically, external disturbances, such as wind, always affect the flight of an aircraft. In order to more accurately model the flare trajectory of a UAV helicopter and the safe region of flare initiation, wind conditions must be taken into account.

1.1 Motivation

Autonomous helicopters represent a promising technology for carrying out reconnaissance, recovery, and evacuation missions due to their ability to hover and operate in tight quarters. While unmanned helicopters have been implemented in certain military applications, developments in the areas of reliability and recoverability could result in their wide-scale use. As missions become more elaborate, the onboard sensor packages required to carry out these missions, such as those on the Northrop Grumman Fire-X, have become more complex, and hence more expensive (several of these helicopters can be seen in Figure 1.1). In an evacuation situation, the loss of payload in the event of failure is an unacceptable outcome, and is a topic that has garnered much attention as the technology has developed. Power loss due to engine failure, transmission problems, or loss of tail rotor control is known to be recoverable through autorotation [1].

(a) Northrop Grumman Fire-X

(b) Boeing Unmanned Little Bird

(c) Lockhead Martin K-MAX

Figure 1.1. Autonomous helicopters. Image credits: [a]: Northrop Grumman; [b]: Boeing; [c]: Lockhead Martin.

Autorotation is an extremely difficult and dangerous maneuver. It is an impre-

cise science, and failure in manned rotorcraft often occurs due to pilot error, and as a result, safety of autorotation continues to be a major concern for the manned rotorcraft community. The final flare phase of autorotation is especially dangerous due to the helicopter's close proximity to the ground, high descent rates, limited stored energy, and the short duration over which the maneuver occurs. A series of precise control inputs are required for a successful landing, and wind disturbances further complicate this process. Practice autorotation continues to be a crucial aspect of the training curriculum for military pilots, but is a dangerous part of the training. A successful autorotation is highly dependent on timing, and thus many accidents occur during practice. While multi-engine aircraft can often compensate for a partial loss of power, most UAV helicopters are single-engine vehicles and remain highly susceptible to engine failure and autorotation.

The wide-scale implementation of autonomous rotorcraft for military and civilian use is dependent on the reliability of the aircraft. In fully autonomous flight, a helicopter must display the ability to recover from engine failure without the loss of payload. Autorotation is an exceedingly difficult maneuver, particularly the flare phase, where real-time trajectory planning is not feasible. A cueing system would be beneficial for both manned and unmanned rotorcraft, which would reduce the pressure placed on the pilot in the case of engine failure in a manned helicopter. In an unmanned helicopter, this system would need to enter into the autorotative maneuver, maintain a steady descent, and flare shortly before touchdown, resulting in a safe landing. This thesis aims to expand upon previous works that focus on the final flare maneuver by investigating the effects of wind on the flare trajectory.

1.2 Stages of a Safe Autorotation

Autorotation is defined as the flight condition a helicopter enters when it loses power to its main rotor. In the event of engine failure, the helicopter begins to descend at a relatively high but controlled rate such that the vehicle's potential energy is traded for kinetic energy used to drive the rotor [1]. In this way, the upflow of air is used to windmill the rotor, generating thrust and providing controllability to the descent of the vehicle. There are four main phases of autorotation: engine failure, entry, steady-state descent, and flare (beginning with flare initiation). The

whole of the autorotation maneuver can be seen in Fig. 1.2.

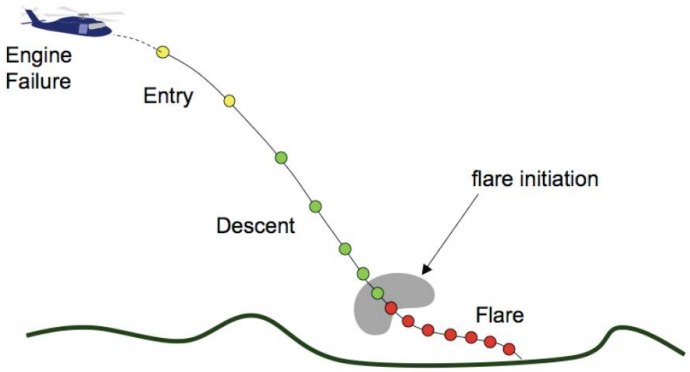

Figure 1.2. Stages of autorotation: engine failure, entry, descent, and flare.

Engine failure results in a rapid loss of power to the main rotor, at which point the pilot must immediately decrease the collective in order to regain rotor RPM. Entry is characterized by changing airspeed and descent rate in order to establish a steady-state glide. This is done by adjusting collective and cyclic pitch as necessary in order to maintain a desired rotor RPM and airspeed. As the helicopter begins to descend, the upflow through the rotor keeps it spinning sufficiently such that thrust and controllability can be maintained at a steady rate. The descent phase of autorotation occurs at steady-state, during which the pilot (or autopilot) must locate an acceptable landing site and set up the vehicle for flare. Once the helicopter has reached the proper altitude above and distance from the desired landing target, it must initiate flare in order to safely land the helicopter.

"Flare", for the purposes of this thesis, is the final portion of an autorotative descent, at which point the helicopter is transitioned from a steady-state flight condition through a series of control inputs in an effort to reduce the velocity of the aircraft to a point that safe touchdown can occur. This involves increasing the collective pitch and adjusting longitudinal cyclic which results in increased thrust and an aft tilting of the thrust vector which counters the forward and vertical speeds of the helicopter on the way to touchdown. Flare is an extremely difficult and dangerous maneuver due to the limited rotational energy stored in the rotor. A change in vehicle pitch attitude, followed by an increase in collective, marks the initiation of flare in an effort to reduce the forward speed and descent rate of

the aircraft, as well as maintain a safe pitch attitude, such that a tail strike does not occur. The rotor kinetic energy, which is a result of rotor speed and inertia, represents the only energy which can be used to control the descent, meaning an increase in collective results in a large buildup of drag and a rapid decrease in rotor speed. Once the rotor speed is bled off it cannot be recovered, and the thrust generated by the main rotor is greatly diminished. For this reason, timing is crucial to a successful flare maneuver. If flare is initiated too early, rotor speed is bled off before touchdown occurs, and the helicopter falls out of the sky. If flare is initiated too late, the helicopter's velocity cannot be reduced sufficiently enough and a crash landing occurs.

This thesis expands upon the work done by Tierney in the development of the *safe landing set*. At the time of flare initiation, the helicopter may be in one of a number of different steady-state descent conditions and positions with respect to the desired landing site. Certain combinations of steady-state conditions and initation points may result in a safe landing. These combinations comprise what is known as the safe landing set. The work of Tierney is described in detail in [2], but in short, the safe landing set is the set of all points in the helicopter's steady-state autorotation space (defined by horizontal speed, descent rate, and rotor speed), combined with height above and distance to the desired touchdown point, from which a safe path to touchdown is guaranteed to exist.

1.3 Flare in Wind Shear

Much of the research done in the area of autorotation path planning (discussed in Section 1.4) assumes ideal conditions; namely there is no wind present and the terrain surrounding the helicopter is flat and obstacle-free. In reality, wind disturbances always influence the flight of an aircraft. This thesis aims to investigate the influence of wind and wind shear on the safe landing set.

The wind profile used is modeled as a two-dimensional, fully developed wind shear profile, seen in Figure 1.3. The wind velocity is assumed to be exclusively in the horizontal direction, and whose magnitude increases logarithmically with altitude. This serves to alter the helicopter's airspeed as it descends through the shear profile. This thesis aims to explore the influence of wind shear on the flare

trajectory of an autonomous helicopter by: (a) incorporating wind into the height-discretized equations of motion presented in [2]; (b) analyzing the influence of wind shear of varying magnitudes, as well as headwind versus tailwind conditions, on individual flare trajectories as well as the safe landing set; (c) presenting safe landing set results for two helicopters: a mid-size utility helicopter and a small-scale UAV helicopter; and (d) generating and testing a full flare trajectory in the simulation environment of the small-scale UAV.

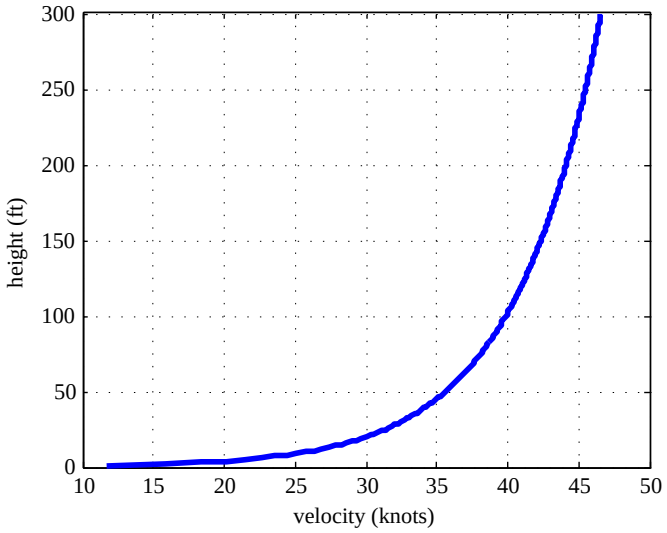

Figure 1.3. Wind shear profile.

1.4 Review of Related Work

There have been previous studies into vehicle recovery through autorotation in the event of engine failure. The entry, descent, and flare phases of autorotation are each active areas of research. There have been investigations into descent phase path planning of unmanned helicopters in the event of engine failure [3,4]. Several researchers have investigated the use of optimal control in order to recover manned helicopters under partial or total power loss [5–8]. Additionally, there have been studies into trajectory planning for fixed-wing and rotorcraft in the event of engine failure [9–12].

The safe landing set, mentioned in Section 1.2, is a backwards reachable set, meaning for any vehicle which enters the safe landing set, a safe, feasible path to touchdown is guaranteed to exist. There have been studies which implement backwards reachable sets for safe, powered landing of fixed-wing aircrafts [13, 14]. Additionally, the work done by Tierney presents the use of backwards reachable sets for landing rotorcraft under power loss.

While these investigations yield promising results, they all assume ideal conditions; namely, no wind and a flat, obstacle-free landing site. This research aims to expand the study of helicopter path planning under power loss by including the effects of wind and wind shear.

1.5 Contributions

The primary contribution of this thesis is the investigation of the influence of wind on the flare phase of autorotation for autonomous helicopters. It defines an altitude-dependent wind shear profile, and its governing equations are incorporated into the longitudinal equations of motion for a generic utility helicopter.

- The effect of wind shear on the safe landing set is described and computed.
- Safe landing sets are computed for two helicopters (the Bell OH-58A and the Adaptive Flight Hornet Mini, a $55''$ rotor diameter unmanned helicopter) through shear profiles representative of light, moderate, and severe head and tailwinds.
- Simulation results: safe flare to landing is demonstrated in the Adaptive Flight Hornet Mini simulation environment using GPS waypoint navigation.

1.6 Reader's Guide

Chapter Two describes the problem that is solved by this thesis. It also defines the shear profile and incorporates wind into the height-discretized equations of motion.

Chapter Three describes the method for using trajectory optimization to find safe paths from flare initiation to landing. It also describes the algorithm used to find the safe landing set, which utilizes trajectory optimization.

Chapter Four shows simulation results of the safe landing set algorithm presented in Chapter Three. It describes the properties of the two helicopters used throughout the simulation. Additionally, it will investigate the influence of shear layers of varying magnitudes as well as the influence of a headwind versus a tailwind on the safe landing set.

Chapter Five describes the generation and testing of flare trajectories using the simulation environment developed by Adaptive Flight. It also gives a more detailed description of the Hornet Mini UAV.

Chapter Six summarizes results and presents conclusions. It also gives recommendations for future work in this area of research.

Chapter 2

The Flare Maneuver Through a Wind Shear Profile

This chapter provides the necessary equations and methods used in developing the results that are given in this thesis. The difficulties of flaring through a shear profile are discussed in Section 2.1. Next, the shear profile model, as given by Military Standard 1797A and used throughout this thesis, is described in Section 2.2. The simplified equations of motion that govern the flight of a helicopter are presented in Section 2.3. The autorotation governing equations and the wind shear equations are each presented. Next, the equations are combined into a single set that govern the autorotation of a helicopter in wind shear. These equations are then converted to height-parameterized equations of motion. Finally, Section 2.4 presents the optimal trajectory generation for flare in wind shear.

2.1 Problem Statement

The scenario under consideration is a helicopter initiating and proceeding through the flare phase of autorotation under the influence of wind shear (Figure 2.1).

Flare initiation consists of transitioning from a steady-state descent to the flare maneuver through the use of control inputs. Initiation is characterized by a set of trimmed autorotation states and an initiation point. The helicopter's trimmed autorotation states include the horizontal and vertical speeds (u and w) and the rotor speed, Ω. The wind velocity at a given altitude is included in the equations of

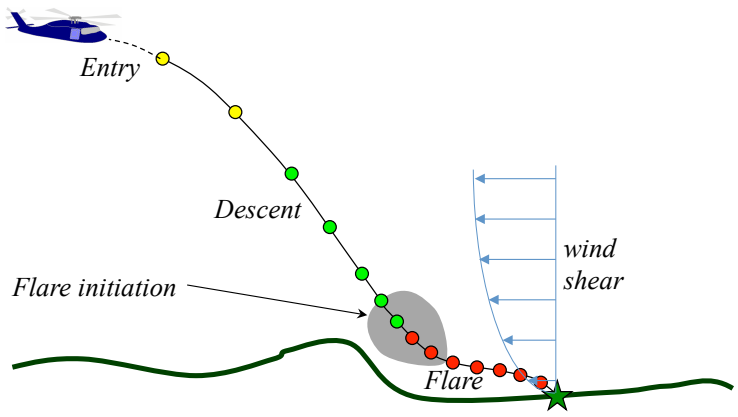

Figure 2.1. Schematic of the autorotation scenario.

motion, making u and w airspeed measurements in the body frame. The initiation point is defined as a distance from and height above the designated touchdown point. Therefore, the state vector can be written as:

$$\mathbf{x} = [u \; w \; \Omega \; x \; h]^T \tag{2.1}$$

For flare analysis, the touchdown point is designated as (x,h) = (0,0). The final touchdown states are bounded by an allowable range of values such that the velocities are low and the vehicle touches down at a position close to the origin.

The control inputs used throughout the flare maneuver are the main rotor thrust coefficient and tip-path-plane angle that correspond to the particular steady-state condition:

$$\mathbf{u} = [C_T \; \alpha]^T \tag{2.2}$$

These inputs are a slight simplification (they ignore actuator dynamics as well as aircraft rotational dynamics), but essentially represent collective and longitudinal cyclic pitch controls, as the total thrust and orientation of the rotor disk are being manipulated. The inputs are used to control the foward and vertical velocities, as well as the rotor speed throughout the maneuver. The velocities in turn control the position of the helicopter. The flare maneuver ends when the helicopter reaches the ground. The height above touchdown, h, is a relative measure of altitude with respect to the landing gear. It is therefore known that touchdown

occurs when $h = 0$.

The problem of computing a safe flare path from the moment of engine failure to touchdown can be expressed as a trajectory optimization problem. In its most general form this can be expressed as:

$$\text{minimize } C \tag{2.3}$$

$$\text{subject to } \dot{\mathbf{x}} = f(\mathbf{x}, \mathbf{u}) \tag{2.4}$$

$$g(\mathbf{x}) \leq 0 \tag{2.5}$$

$$\mathbf{x}(t = 0) = \mathbf{x}_0 \tag{2.6}$$

C is a cost function dependent on vehicle states during flare and at touchdown; $\dot{\mathbf{x}} = f(\mathbf{x}, \mathbf{u})$ are the equations of motion; $g(\mathbf{x})$ represents state dependent constraints such as structural loads or aircraft performance limits.

Headwind and tailwind conditions will influence the trajectory of the helicopter during flare. This is because the magnitude of the wind velocity decreases as the helicopter descends. This change in wind speed affects the helicopter's airspeed, which in turn affects the descent rate, the rotor inflow, and the rate of change of rotor speed. Since the helicopter is in autorotation, no power can be supplied from the engine and there is limited energy stored in the rotor to arrest the helicopter's velocity. Thus, headwinds and tailwinds of varying magnitudes will alter the region of the steady-state autorotation space from which a safe path to touchdown exists.

2.2 Defining the Shear Profile

The main focus of the shear analysis is horizontal winds, specifically the change in horizontal wind speed with altitude. A logarithmic shear profile is defined in MIL-STD-1797A [15]:

$$w_x = u_{20} \frac{\ln(\frac{h}{z_0})}{\ln(\frac{20}{z_0})} \tag{2.7}$$

Here, u_{20} represents the wind velocity at 20 feet above the ground and z_0 represents the surface roughness. Figure 2.2 shows the shear profiles for u_{20} values of 10-knot, 30-knot, and 45-knot wind conditions. In all cases $z_0 = 0.15$. This

surface roughness value is presented in [15] and is used for approach and landing flight situations.

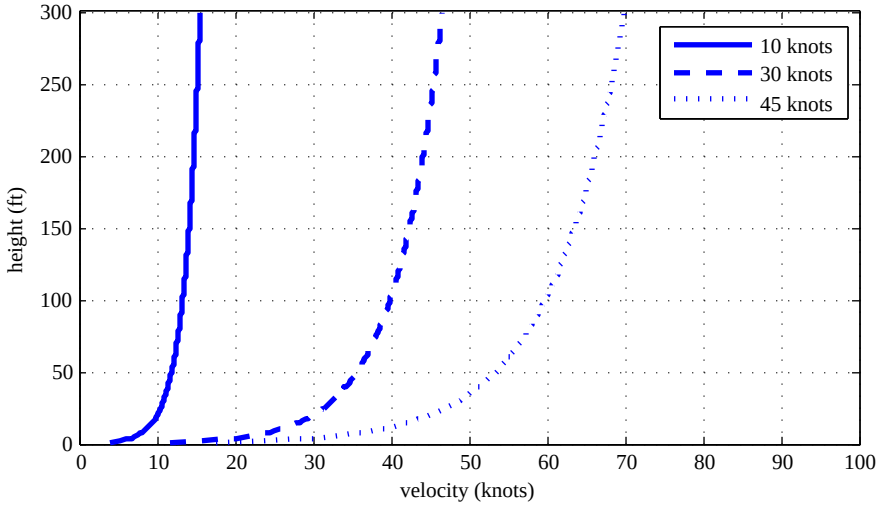

Figure 2.2. Wind shear profiles for light, moderate, and severe wind conditions.

This model of wind shear is accurate for relatively low altitudes. This makes it suitable for the work presented in this thesis due to the low altitudes at which flare is generally initiated. Its mathematical representation allows it to be added to existing equations of motion in order to model airspeed. Additionally, it can be explicitly modeled as a headwind or a tailwind of varying magnitudes by adjusting the value of u_{20}.

Three shear profile strengths are outlined in [15]: light, moderate, and severe. These profile strengths are defined by the wind velocity at 20 feet, and Equation (2.7) is used to generate the profile. The u_{20} values and the probability of exceeding those values are presented in Table 2.1.

Table 2.1. Wind Shear Profile Intensity

Wind Condition	**Velocity at 20 feet**	**Probability of Exceedance**
Light	0 - 10 knots	10%
Moderate	11 - 30 knots	0.1%
Severe	31 - 45 knots	0.001%

2.3 Equations of Motion

This section presents the equations of motion used to calculate the safe landing set in wind shear. First, the governing equations for a helicopter in autorotation are presented in Section 2.3.1. Next, the equations that define the shear profile are described in Section 2.3.2, and are then incorporated into the autorotation equations in Section 2.3.3. Finally, the complete equations of motion for a helicopter operating in wind shear are height-discretized in Section 2.3.4.

Flare occurs very quickly and very close to the ground. Because of the difficulty of the maneuver, lateral motion of the helicopter is generally avoided. For this reason, the flare trajectory is modeled as a two-dimensional path. Additionally, the helicopter is represented by a point-mass with a main rotor, for which all forces act at a localized point below the rotor hub.

2.3.1 Autorotation Governing Equations

Equations for a point mass model of a helicopter in autorotation operating in zero wind are given by Aponso [16]. These equations can be extended to include the effects of time- or spatially-varying wind:

$$\dot{u} = \frac{1}{m}\left[\rho(\pi R^2)(\Omega R)^2 C_x - \frac{1}{2}\rho f_e u\sqrt{u^2+w^2}\right] + \dot{w}_x \tag{2.8}$$

$$\dot{w} = \frac{1}{m}\left[mg - \rho(\pi R^2)(\Omega R)^2 C_z - \frac{1}{2}\rho f_e w\sqrt{u^2+w^2}\right] + \dot{w}_z \tag{2.9}$$

$$I_R\Omega\dot{\Omega} = P_s - \frac{1}{\eta}\rho(\pi R^2)(\Omega R)^3 C_P \tag{2.10}$$

$$\dot{x} = u + w_x \tag{2.11}$$

$$\dot{h} = -(w + w_z) \tag{2.12}$$

$$\dot{P}_s = \frac{1}{\tau_p}(P_{res} - P_s) \tag{2.13}$$

One thing to note is the overloaded symbols used in the governing equations: w denotes helicopter descent rate (with respect to the air mass) and $\mathbf{w} = [w_x\ w_z]^T$ denotes the wind vector and its components in the horizontal and vertical directions. Additionally, u denotes helicopter horizontal speed (with respect to the air

mass) and u_{20} (which defines the wind shear) denotes wind speed 20 feet above the ground.

The work presented here deals with the flare phase of autorotative descent. For this reason, it can be assumed that the residual power, P_{res}, has decayed away to zero during the steady descent phase. Equation (2.13) then simplifies to the identity $0 = 0$. Note that the equations originally presented by Lee [17] explicitly include aircraft pitch angle, θ, as a state. However, Aponso assumes $\theta \approx \alpha$, and the same assumption is made in this thesis as well. Tip-path-plane angle is then used in place of pitch angle, and coefficients are defined as:

$$C_P = \frac{1}{8}\sigma c_{d0} + C_T\lambda \tag{2.14}$$

$$C_x = C_T \sin\alpha \tag{2.15}$$

$$C_z = C_T \cos\alpha \tag{2.16}$$

$$\lambda = \frac{u\sin\alpha - w\cos\alpha + v}{\Omega R} \tag{2.17}$$

The induced velocity is given as:

$$v = K_{ind} v_h f_I f_G \tag{2.18}$$

where v_h is the hover induced velocity, f_I is the ratio of actual induced velocity to the hover induced velocity, and f_G accounts for the decrease in induced velocity due to ground effect:

$$v_h = (\Omega R)\sqrt{\frac{C_T}{2}} \tag{2.19}$$

$$f_I = \begin{cases} 1/\sqrt{b^2 + (a + f_I)^2} & if (2a+3)^2 + b^2 \geq 1 \\ a(0.373a^2 + 0.598b^2 - 1.991) & otherwise \end{cases} \tag{2.20}$$

$$f_G = 1 - \frac{R^2\cos^2\theta_w}{16(h + H_R)^2} \tag{2.21}$$

$$\cos^2\theta_w = \frac{(-wC_T + vC_z)^2}{(-wC_T + vC_z)^2 + (uC_T + vC_x)^2} \tag{2.22}$$

a and b are given as:

$$a = \frac{u \sin\alpha - w \cos\alpha}{v_h} \tag{2.23}$$

$$b = \frac{u \cos\alpha + w \sin\alpha}{v_h} \tag{2.24}$$

It now remains to compute the components of the rate of change of wind speed.

2.3.2 Wind Shear Equations of Motion

The total time derivative of wind contains both a time rate of change and the change induced by helicopter motion through a spatial gradient:

$$\frac{d\mathbf{w}}{dt} = \begin{bmatrix} \frac{\partial w_x}{\partial t} \\ \frac{\partial w_z}{\partial t} \end{bmatrix} + \begin{bmatrix} \frac{\partial w_x}{\partial x} & \frac{\partial w_x}{\partial h} \\ \frac{\partial w_z}{\partial x} & \frac{\partial w_z}{\partial h} \end{bmatrix} \begin{bmatrix} u \\ w \end{bmatrix} \tag{2.25}$$

As previously mentioned, the shear model being used assumes that there is no component of wind in the z direction. Therefore, $w_z = 0$ and

$$\dot{w}_x = \frac{\partial w_x}{\partial t} + \begin{bmatrix} \frac{\partial w_x}{\partial x} & \frac{\partial w_x}{\partial h} \end{bmatrix} \begin{bmatrix} u \\ w \end{bmatrix} \tag{2.26}$$

Additionally, it is assumed that wind does not vary with time and there is no gradient in the horizontal direction. Therefore, Equation (2.26) can be further reduced to:

$$\dot{w}_x = \frac{\partial w_x}{\partial h} w \tag{2.27}$$

Incorporating Equation (2.7), and the total rate of change of wind can be written as:

$$\dot{w}_x = \frac{u_{20}}{\ln\left(\frac{20}{z_0}\right)} \frac{w}{h} \tag{2.28}$$

2.3.3 Incorporating Wind Shear

The equations of motion for a helicopter in autorotation are now combined with the shear equations. Since the shear layer is restricted to wind velocities only in the horizontal direction, only two of the equations from Aponso are amended. The rest remain unchanged.

$$\dot{u} = \frac{1}{m}\left[\rho(\pi R^2)(\Omega R)^2 C_x - \frac{1}{2}\rho f_e u\sqrt{u^2+w^2}\right] + \frac{u_{20}}{\ln\left(\frac{20}{z_0}\right)}\frac{w}{h} \tag{2.29}$$

$$\dot{w} = \frac{1}{m}\left[mg - \rho(\pi R^2)(\Omega R)^2 C_z - \frac{1}{2}\rho f_e w\sqrt{u^2+w^2}\right] \tag{2.30}$$

$$I_R\Omega\dot{\Omega} = P_s - \frac{1}{\eta}\rho(\pi R^2)(\Omega R)^3 C_P \tag{2.31}$$

$$\dot{x} = u + u_{20}\frac{\ln(\frac{h}{z_0})}{\ln(\frac{20}{z_0})} \tag{2.32}$$

$$\dot{h} = -w \tag{2.33}$$

During the flare phase of autorotation, descent rate w is typically positive. In a head wind, u_{20} is negative (see Equation (2.32) for this sign convention). Equation (2.29) shows (and all pilots can attest) that for a helicopter descending through headwind shear, airspeed will decrease more rapidly than it would for descent in zero wind. This complicates the problem of safe flare, with high wind speeds (u_{20}) increasing the difficulty. Conversely, the opposite would occur for descent through tailwind shear, but in that case the problem would be excessive ground speed.

2.3.4 Height-Parameterized Equations of Motion

The flare maneuver is dependent on an input sequence, $\mathbf{u}(t)$, that is used to control the helicopter's trajectory during the descent. These input controls manipulate the helicopter states in order to generate a path to touchdown without violating operational bounds. In order to solve the problem, the path is discretized into small, finite steps in order to maintain the assumption that the control input is constant over each step. This results in a parameter optimization problem. Generally, opti-

mization problems are time-dependent such that $\mathbf{t} = [t_0\ t_1\ t_2 ... t_k ... t_{final}]$ is a vector of equally spaced times whose values are known.

The difficulty with the flare problem is that it is highly dependent on the control sequence, which is constantly changing. The time between flare initiation and touchdown is dictated by the initiation height and the descent rate. C_T and α variations change the descent rate, meaning that the time of touchdown, t_{final}, is not known until it is reached. One solution is to discretize the problem in terms of height, making time an additional parameter. This simplifies the problem because touchdown is known to occur when $h = 0$, regardless of initial states or control inputs.

Tierney presents a methodology for converting to height-parameterized equations of motion based on a forward Euler integration [2], seen in Figure 2.3.

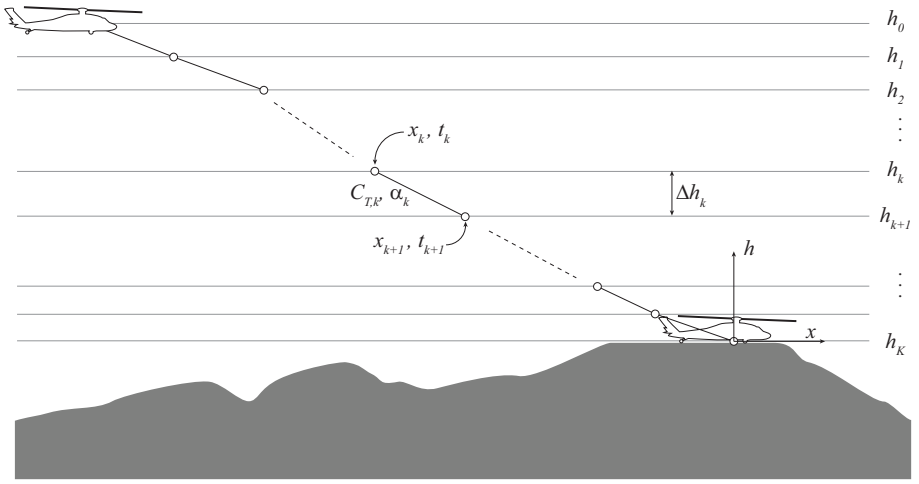

Figure 2.3. Schematic of the height-discretized flare trajectory optimization problem. The target touchdown point is at the origin, the shaded region denotes terrain [2].

Using this approach, height above touchdown becomes the independent variable, and time becomes a dependent variable, making the state vector:

$$\mathbf{x} = [\ u\ w\ \Omega\ x\ t\ ]^T \tag{2.34}$$

The height-discretized equations of motion for autorotation descent of a helicopter through wind shear can now be written as:

$$\mathbf{x}_{k+1} = \mathbf{x}_k + \left.\frac{d\mathbf{x}}{dh}\right|_k \Delta h_k \tag{2.35}$$

where the components of $\frac{d\mathbf{x}}{dh}\big|_k$ (including the effects of wind shear) are

$$\frac{du}{dh} = -\frac{1}{mw}\left[\rho(\pi R^2)(\Omega R)^2 C_x - \frac{1}{2}\rho f_e u\sqrt{u^2+w^2}\right] - \frac{u_{20}}{\ln\left(\frac{20}{z_0}\right)}\frac{1}{h} \tag{2.36}$$

$$\frac{dw}{dh} = -\frac{1}{mw}\left[mg - \rho(\pi R^2)(\Omega R)^2 C_z - \frac{1}{2}\rho f_e w\sqrt{u^2+w^2}\right] \tag{2.37}$$

$$\frac{d\Omega}{dh} = -\frac{1}{I_R\Omega_w}\left[P_s - \frac{1}{\eta}\rho(\pi R^2)(\Omega R)^3 C_P\right] \tag{2.38}$$

$$\frac{dx}{dh} = -\frac{u}{w} - \frac{u_{20}}{w}\frac{\ln\left(\frac{h}{z_0}\right)}{\ln\left(\frac{20}{z_0}\right)} \tag{2.39}$$

$$\frac{dt}{dh} = -\frac{1}{w} \tag{2.40}$$

This approach has two implicit assumptions: first, descent rate is always positive (i.e. the helicopter cannot "swoop" upwards); second, the time interval Δt_k, is short enough that the descent rate over that interval is constant [2].

2.4 Optimal Trajectory Generation for Flare in Shear

In order to generate a flare trajectory, a set of vehicle states is combined with an initiation point, which define flare initiation. The helicopter is assumed to be flying through a wind shear layer, whose magnitude and direction are known prior to flare. Upon initiation, the trajectory is generated by altering the thrust coefficient and tip-path-plane angle throughout the maneuver. The control sequence is height-discretized such that $\mathbf{u} = [u(h_1)\ u(h_2)\ldots u(h_{K-1})]$. This serves to alter the vehicle states, which are calculated at each height step using the equations of motion defined in Section 2.3.4. The path is optimized by minimizing a cost function dependent on vehicle states and controls. Thus, the optimization problem can be summarized as:

$$\text{minimize } C(\mathbf{x}_{0\ldots K}, \mathbf{u}_{0\ldots K-1}) \tag{2.41}$$

$$\text{subject to } \mathbf{x}_{k+1} = \mathbf{x}_k + \left.\frac{d\mathbf{x}}{dh}\right|_k \Delta h_k \tag{2.42}$$

$$\mathbf{x}_{min} \leq \mathbf{x}_k \leq \mathbf{x}_{max} \tag{2.43}$$

$$g(\mathbf{x}_k) \leq 0 \tag{2.44}$$

$$\mathbf{u}_{min} \leq \mathbf{u}_k \leq \mathbf{u}_{max} \tag{2.45}$$

$$\mathbf{x}_0 = [\ u_0\ w_0\ \Omega_u\ x_0\ t_0\ ] \tag{2.46}$$

The cost function is subject to constraints which are dictated by the helicopter's operation limitations. Those constraints are the vehicle height-based equations of motion, state-dependent constraints, and vehicle control limits. The vehicle states at each height step are calculated using the states at the previous step and the height-dependent equations of motion. The state dependent constraints, $g(x)$, include considerations such as structural limitations. The control limits are determined based on vehicle model restrictions.

This process is repeated for numerous combinations of states and initiation points in an effort to produce the safe landing sets for different wind conditions.

2.5 Summary

Section 2.1 defines the problem. The problem involves a helicopter initiating and proceeding through the flare phase of autorotation in the presence of wind shear. Flare initiation is the transition from a steady-state descent to the flare maneuver using control inputs. These controls are used throughout the maneuver in order to manipulate the vehicle states and guide it to a safe landing. The helicopter is modeled as a two-dimensional point-mass with a rotor, and whose states are forward speed, descent rate, and rotor speed. Flare initiation is defined by the helicopter states and associated horizontal distance from and height above the designated landing site. Wind speed is included in the equations of motion, meaning forward speed and descent rate are measures of airspeed in the body frame. Useable control inputs are the main rotor thrust coefficient and tip-path-plane angle that correspond to the steady state condition. Flare begins at initiation, and ends with skid touchdown ($h = 0$) at a designated landing site without violating operational bounds.

The problem is solved using optimal path planning under the influence of various wind conditions. Different wind magnitude and directions (headwind versus tailwind) are investigated.

Section 2.2 defines the shear profile used throughout this thesis. The model is a height-dependent function that increases logarithmically with altitude. The wind velocity at 20 feet is used to define the magnitude of the profile. The model is accurate for relatively low altitudes and can be seamlessly incorporated into existing equations of motion. Additionally, the wind magnitude and direction can be easily adjusted to simulate different wind conditions.

Section 2.3 discusses the equations of motion used throughout the analysis.

Section 2.3.1 discusses the time-discretized equations that govern the flight of a helicopter in autorotation. These equations are given by Aponso and used by Tierney to create the safe landing set. A simplification is made by assuming that the helicopter has been in autorotation long enough that all residual power has been bled off.

Section 2.3.2 presents the derivation of the equations that dictate wind shear. This application of the shear model assumes that there is no component of wind in the vertical direction. Additionally, the wind profile does not vary with time and there is no gradient in the horizontal direction.

Section 2.3.3 incorporates wind shear by combining the equations of motion for autorotation with the equations that define the components of wind shear.

Section 2.3.4 transforms the time-based equations of motion to height-based equations of motion using the method presented by Tierney. This is done because the touchdown time is unknown until it is reached, but touchdown is known to occur when $h = 0$, regardless of initial states or control inputs. This process transforms the trajectory optimization problem into a parameter optimization problem.

Section 2.4 introduces the optimization method used to generate flare trajectories under the influence of the different wind conditions. The control inputs are height-discretized and are used to manipulate vehicle states, which are updated at each height step using the height-discretized equations of motion. The trajectory is optimized by minimizing a cost function, and this process is repeated for different combinations of vehicle states and initiation points in order to generate the safe landing set.

A more detailed methodology for determining the safe landing set in different wind conditions is presented in Chapter 3. Chapter 4 presents results of the safe landing set algorithm for a mid-size utility helicopter and a small-scale UAV helicopter. Chapter 5 presents implementation results of the path planning algorithm in the simulation environment of the small-scale UAV.

Chapter 3

Computing the Safe Landing Set

This chapter describes the methodology for computing the safe landing set for a helicopter operating in wind shear during the flare phase of autorotation. It is presented as a trajectory optimization problem whose algorithm is an extension of the work developed by Tierney. This thesis expands that work by directly incorporating wind into the airspeed measurement and by adjusting the problem parameters to the specifications of the two helicopters discussed later in this chapter. The safe landing set is determined for multiple wind magnitude and direction (headwind versus tailwind) combinations. Each set is found by repeatedly solving the trajectory optimization problem for various combinations of initial conditions.

3.1 The Safe Landing Set

As introduced by Tierney, the safe landing set is the region in the helicopter's state space from which a safe flare path to landing is guaranteed to exist. The state space is restricted to include only steady-state autorotation conditions, $[u\ w\ \Omega]^T$. The vehicle states, combined with initiation points, $[x\ h]$, from which a safe path to touchdown exists, make up the safe landing set.

The safe landing set is a backwards reachable set, meaning a safe, feasible path to touchdown is guaranteed to exist for any vehicle which enters the safe landing set. A helicopter in the descent phase of autorotation can thus use the safe landing set as a target set of states from which to initiate flare that will result in the highest likelihood of a safe landing.

Given the vehicle state

$$\mathbf{x} = [\ u\ w\ \Omega\ x\ h\ ]^T \tag{3.1}$$

where $[u\ w\ \Omega]^T$ are taken from the set of all trimmed autorotation conditions

$$\mathcal{A} = \{\mathbf{a}_i | \mathbf{a}_i = [u\ w\ \Omega]^T\} \tag{3.2}$$

the *safe landing set* is defined as

$$\mathcal{S} = \{\mathbf{s}_i | \mathbf{s}_i = [u\ w\ \Omega\ x\ h]^T, [u\ w\ \Omega]^T \in \mathcal{A}\} \tag{3.3}$$

In Equation (3.3), $\mathbf{s}_i \in \mathcal{S}$ means that there exists a safe flare path that is initiated from $\mathbf{s}_i$. Thus any trajectory that guides the helicopter from the moment of engine failure into $\mathcal{S}$ is guaranteed to end in a safe landing at a particular designated touchdown location [2].

3.2 Trajectory Optimization

The goal of the safe set algorithm is to generate the safe landing set: the set of all points in the helicopter's steady-state autorotation space, combined with flare initiation points, for which a safe, feasible path to touchdown is guaranteed to exist. Individual trajectories are computed by altering the control inputs, $\mathbf{u}(t)$ throughout the maneuver. Assuming that the inputs are constant over some interval results in a parameter optimization problem. The problem is discretized in terms of height, which is useful since the control inputs alter the descent rate at each step, making the touchdown time unpredictable. However, touchdown is known to occur when $h_f = 0$, regardless of inputs or initial states. The trajectory is optimized by minimizing a cost function that is dependent on the helicopter states and controls at each height step.

The cost function, $\mathbf{C}(x, u)$, is a weighted sum of the touchdown and state costs:

$$C(\mathbf{x}_{0\ldots K}, \mathbf{u}_{0\ldots K-1}) = C_{td} + \gamma C_{state} \tag{3.4}$$

where γ is a parameter that adjusts the relative weight of the state cost versus

the touchdown cost.

3.2.1 State Cost

Throughout the maneuver the states are bounded by operational constraints. These constraints can be expressed as a barrier function:

$$c(x) = \frac{1}{(x - x_{min})^2} + \frac{1}{(x_{max} - x)^2} \tag{3.5}$$

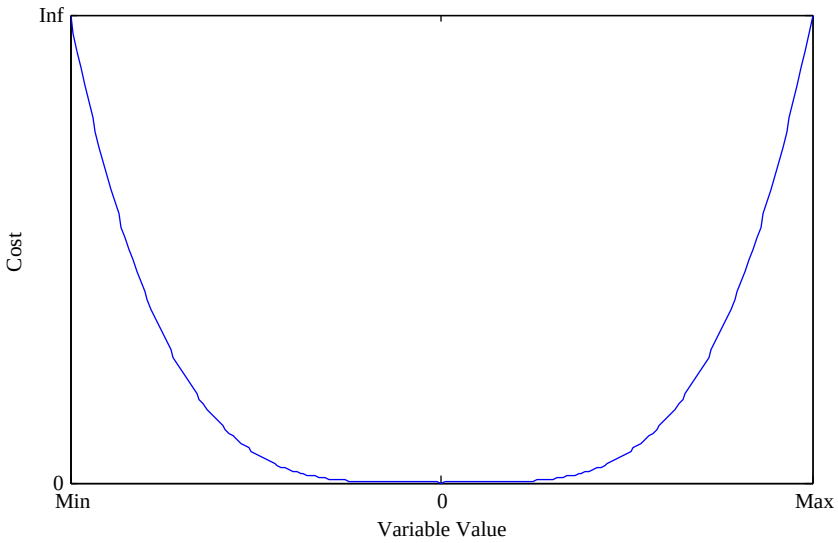

Figure 3.1. Sample barrier function.

The values of x_{min} and x_{max} are dictated by vehicle-specific limitations as well as wind conditions. At any point in the trajectory, the helicopter must be moving towards the target. This requires that the horizontal ground speed be positive. The horizontal speed and descent rate of the helicopter are measured as airspeeds, since they incorporate wind. Therefore, the lower limit of airspeed is equal to the wind velocity. When flying into a headwind, for example, the vehicle airspeed must be at least equal to the wind speed in order to achieve a positive ground speed. The shear profile is a function of altitude, so the values of x_{min} are constantly changing.

The state cost is calculated at each step along the path. The total state cost is equal to the sum of the cost of state violations at each height step:

$$C_{state} = \sum_{k=1}^{K} c(\mathbf{x}_k) \tag{3.6}$$

Once the helicopter is sufficiently close to the ground, landing is assumed to be imminent (the altitude at which this occurs is helicopter-specific). Once the vehicle has reached this altitude, the constraint on rotor speed is dropped. The constraint exists throughout the descent to ensure that the helicopter maintains enough rotor speed to provide lift. Below this altitude, touchdown will occur before the rotor speed can drop off sufficiently enough to degrade the lift.

3.2.2 Touchdown Cost

The touchdown cost is determined by the helicopter states when $h = 0$. The landing site is established as a bounded region on either side of the origin (0,0). The touchdown cost is defined as:

$$C_{td} = \left(\begin{bmatrix} \mathbf{x}_K \\ \mathbf{u}_k \end{bmatrix} - \begin{bmatrix} \mathbf{x}_{des} \\ \mathbf{u}_{des} \end{bmatrix} \right)^T \mathbf{W}_{td} \left(\begin{bmatrix} \mathbf{x}_K \\ \mathbf{u}_k \end{bmatrix} - \begin{bmatrix} \mathbf{x}_{des} \\ \mathbf{u}_{des} \end{bmatrix} \right) \tag{3.7}$$

where $\begin{bmatrix} \mathbf{x}_{des} \\ \mathbf{u}_{des} \end{bmatrix}$ is the desired landing condition, and W_{td} is the touchdown weight matrix.

$$\mathbf{W}_{td} = \text{diag}\left(W_u,\ W_w,\ 0,\ W_d,\ 0,\ 0,\ W_\alpha\right) \tag{3.8}$$

The touchdown cost is dependent only on the proximity to the landing site, the forward speed and descent rate at touchdown, and the aircraft pitch angle at touchdown. When touchdown occurs ($h = 0$), the helicopter landing gear has reached the ground. However, airspeed is measured from the center of gravity of the vehicle, meaning a component of wind is still acting on the helicopter when touchdown occurs. This means that the landing condition of u is dependent on wind velocity in order to achieve a ground speed within a safe range for touchdown.

Specific landing conditions for the utility helicopter and the small UAV are listed in Section 4.4.1 and Section 4.5.1 respectively.

3.2.3 Optimization

The individual trajectories of a landing set for a specific wind condition are calculated by repeatedly solving the optimization problem for a particular initial condition. MATLAB's *fmincon* function, which finds the minimum of a constrained nonlinear multivariable function, is used to optimize the trajectory by minimizing the cost function. The generated solution is a local minimum which satisfies the requirements of a "safe" solution. In order to avoid being trapped in a poor local minima which does not yield a safe solution, the initial guess of control inputs is important.

The control inputs are represented by a five-point spline. The initial guess of thrust coefficient is brought from its trimmed condition to its maximum value, which maximizes thrust near touchdown to reduce descent rate. The tip-path-plane angle is brought from its trimmed condition to a high negative value and then back down to the terrain level. This enables the helicopter to "sprint" to the landing site before decelerating during landing.

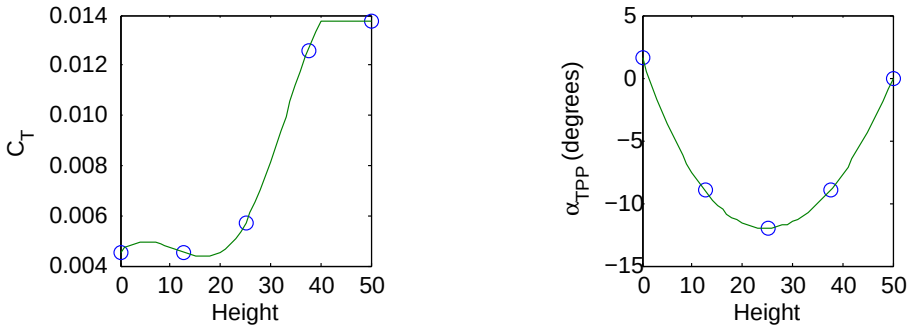

Figure 3.2. Control Spline Initial Guess

The optimization problem can now be written more specifically as:

$$\text{minimize } C_{td} + \gamma C_{state} \tag{3.9}$$

$$\text{subject to } \mathbf{x}_{k+1} = \mathbf{x}_k + \left.\frac{d\mathbf{x}}{dh}\right|_k \Delta h_k \tag{3.10}$$

$$\mathbf{x}_{min} \leq \mathbf{x}_k \leq \mathbf{x}_{max} \tag{3.11}$$

$$g(\mathbf{x}_k) \leq 0 \tag{3.12}$$

$$\mathbf{u}_{min} \leq \mathbf{u}_k \leq \mathbf{u}_{max} \tag{3.13}$$

$$\mathbf{u}_k = spline(U) \tag{3.14}$$

$$x_0 = [\ u_0\ w_0\ \Omega_0\ d_0\ t_0\ ] \tag{3.15}$$

To find a solution, the first iteration uses a large value of γ to generate a path that does not violate state constraints. If a path is found, then γ is decreased in an effort to minimize the cost function, using the previous solution as an initial guess. This process is repeated until a path that is both feasible and safe (touchdown constraints are not violated) is found. If a trajectory is found that violates the state constraints, then γ is increased and the process is repeated.

3.3 Safe Set Algorithm

For a specific wind condition, the safe landing set, $\mathcal{S}$, is found by repeatedly solving the optimization problem for various combinations of states and initiation points. Any combinations that result in a safe landing are members of the safe landing set. Throughout the maneuver, the states and controls are monitored to ensure that they do not violate state constraints. These constraints are dependent on the wind velocity and operational restrictions of the helicopter. At touchdown, the final states are examined to ensure that they lie within boundaries that constitute a "safe landing". If any of the state or touchdown constraints are violated throughout the path, the maneuver is considered a failure.

Candidate initial states are members of a trimmed set of steady-state autorotation conditions

$$\hat{\mathbf{s}}_i = \left[x_{ip}\ h_{ip}\ \mathbf{a}_i^T\right]^T,\ \mathbf{a}_i \in \mathcal{A} \tag{3.16}$$

where $\mathcal{A}$ is the set of all trim conditions for the helicopter under consideration.

Various members of this set are tested at each initiation point in the flare region of the helicopter. If the states result in a safe, feasible path to touchdown, then those states and the corresponding point at which the flare was initiated are a part of the safe landing set ($\hat{\mathbf{s}} \in \mathcal{S}$). The procedure is summarized in Algorithm 1.

The various safe landing sets for the different wind conditions were generated

Algorithm 1 Computing the safe landing set.

1: Define wind severity, u_{20}
2: $\mathcal{S} = \emptyset$
3: Select candidate $\hat{\mathbf{s}}_i = \left[x_{ip}\ h_{ip}\ \mathbf{a}_i^T\right]^T$
4: Compute optimal trajectory from $\hat{\mathbf{s}}_i$ to goal
5: **if** trajectory is feasible and safe **then**
6: $\quad \mathcal{S} = [\mathcal{S}\ \hat{\mathbf{s}}_i]$
7: **else if** Trajectory is feasible but not safe **then**
8: $\quad$ reduce γ
9: $\quad$ go to 4
10: **else if** Trajectory is safe but not feasible **then**
11: $\quad$ increase γ
12: $\quad$ go to 4
13: **else**
14: $\quad$ discard $\hat{\mathbf{s}}$
15: **end if**
16: **if** No more candidate states **then**
17: $\quad$ Return $\mathcal{S}$
18: **else**
19: $\quad$ go to 3
20: **end if**

for two helicopters: the Bell OH-58A and Adaptive Flight's Hornet Mini (seen in Figure 3.3).

(a) OH-58 (b) Hornet Mini

Figure 3.3. Helicopters used in flare analysis.

Due to the high number of candidate flare initiation combinations, the safe set algorithm is very time consuming to run. This process can be expedited using MATLAB's parallel computing toolbox, which maximizes the number of cores used to evaluate the problem. This can significantly reduce run time, which is beneficial

when generating safe landing sets for multiple wind conditions.

3.4 Summary

This chapter introduces a methodology for computing the safe landing set. Section 3.1 summarizes the safe landing set. The safe landing set is a backwards reachable set of steady-state conditions and initiation positions from which a safe path to touchdown is guaranteed to exist. Candidate initial states are taken from the set of all trimmed autorotation conditions.

Section 3.2 describes how trajectory optimization is used to generate safe flare paths to touchdown. The individual trajectories are optimized by minimizing a cost function, C, which is a weighted sum of the state cost and the touchdown cost.

Section 3.2.1 describes the state cost, C_{state}, which is modeled as a barrier function. Throughout the maneuver, the states are bounded by operational constraints and wind conditions. The vehicle must always be moving towards the target, meaning the ground speed must be positive. The lower limit on airspeed is therefore dictated by wind velocity. The total state cost is equal to the sum of state violations at each height step.

Section 3.2.2 introduces the touchdown cost, C_{td}. The touchdown cost is dependent only on vehicle position, forward speed, descent rate, and pitch angle at touchdown. Landing occurs when $h = 0$, or when the skids contact the ground; however wind acts on the center of gravity of the vehicle, meaning a component of wind is still acting on the helicopter at touchdown. Thus, wind speed dictates the forward airspeed limitation upon landing.

Section 3.2.3 describes the gradient-based approach used to optimize flare trajectories. MATLAB's *fmincon* function is used to minimize the cost function. The solution is a local minimum which is highly dependent on the initial guess of control inputs. The optimizer uses an iterative approach which alters the coefficient, γ, in order to adjust the relative weight between the state cost and the touchdown cost.

Section 3.3 describes the algorithm used to generate the safe landing set. The safe landing set is found by repeatedly solving the optimization problem for differ-

ent combinations of states and initiation points. Any combinations that result in a safe landing are members of the safe landing set. This process is repeated for various wind conditions. The safe landing sets are generated for two helicopters: the Bell OH-58 and the Adaptive Flight Hornet Mini. The OH-58 was chosen due to its similarities to the Northrop Grumman Fire-X and the availability of its vehicle properties. The Hornet Mini is a small scale autonomous helicopter that is useful for testing flare trajectories both in simulation and in hardware implementation.

Chapter 4 presents simulation results for the algorithm discussed in this chapter. The safe landing sets are generated for light, moderate, and severe headwinds and tailwinds, in an effort to locate a common region of initial states.

Chapter 4

Safe Landing Set Simulation Results

This chapter shows the safe landing sets that were generated for the OH-58 and the Hornet Mini under varying wind conditions. First, the algorithm used to generate the safe landing set is briefly reviewed. The properties of the two helicopters are then outlined and the safe landing sets are shown for light, moderate, and severe headwinds and tailwinds, as well as a zero wind condition. Finally, trajectory and state history comparisons are shown in order to demonstrate the influence of wind shear on the flight of the helicopter.

4.1 Simulation Approach

The safe landing sets were generated for both helicopters under wind conditions that ranged from severe tailwinds through severe headwinds. The algorithm used to generate the safe landing sets is outlined in Chapter 3. The flare region is defined as the range of position values with respect to the landing site from which the helicopter can realistically flare and land. The region is represented as a series of discrete points defined by distance and height measurements away from the origin. Different sets of steady-state flight conditions, composed of forward speed, descent rate, and rotor speed, are tested at each initiation point in the flare region. Any combinations that result in a safe landing are members of the safe landing set; a safe path to touchdown is guaranteed to exist if flare is initiated using this set of states. This process is repeated for different wind shear profiles.

The algorithm, developed by Tierney, optimizes individual flare trajectories

using MATLAB's *fmincon* function. The control vector, $\mathbf{u}$, is represented by a 5-point spline and is optimized over the trajectory in order to safely land the helicopter. The vehicle controls are subject to operation constraints: the thrust coefficient has an upper limit of $1.5C_w$ (where C_w is the vehicle weight coefficient) and a lower limit of 1e-4, and the tip-path-plane angle is bounded between $+30°$ and $-30°$. The function is given a maximum of 20 iterations to find a minimum cost. If a safe and feasible path to touchdown is found, the control sequence is saved and the vehicle states are marked as a member of the safe landing set.

4.2 Visualizing the Safe Landing Set

The safe landing set can be difficult to visualize due to the high dimensionality of the problem: the state vector is five-dimensional. One way to effectively visualize the safe set is by using parallel coordinates, shown in Figure 4.1. Parallel coordinates offer a means of displaying the region of the autorotation space that results in a safe landing. Each state occupies its own coordinate along the x-axis. The various state and position values that result in a safe landing are scaled by the corresponding maximum tested value of each state. This allows for the display of the different states on the same sized axes without skewing the image.

The grey area represents the bounded region of the safe landing set for the OH-58 acting in zero wind. All combinations of states that result in a safe landing live within this bounded region. Two of these combinations can be seen as the blue and green lines in Figure 4.1. These lines represent the state combinations of the two safe landings that occurred at the initiation point where $d = -230$ feet and $h = 190$ feet. As can be seen, the d and h values are the same for the two conditions, since they both occurred at the same flare initiation point. The state values then branch off, each branch representing a different steady-state autorotation descent condition within the bounded region.

4.3 Various Cases for Headwinds and Tailwinds

The safe landing sets for each helicopter were generated under the influence of light, moderate, and severe headwinds and tailwinds, as well as a zero wind condition.

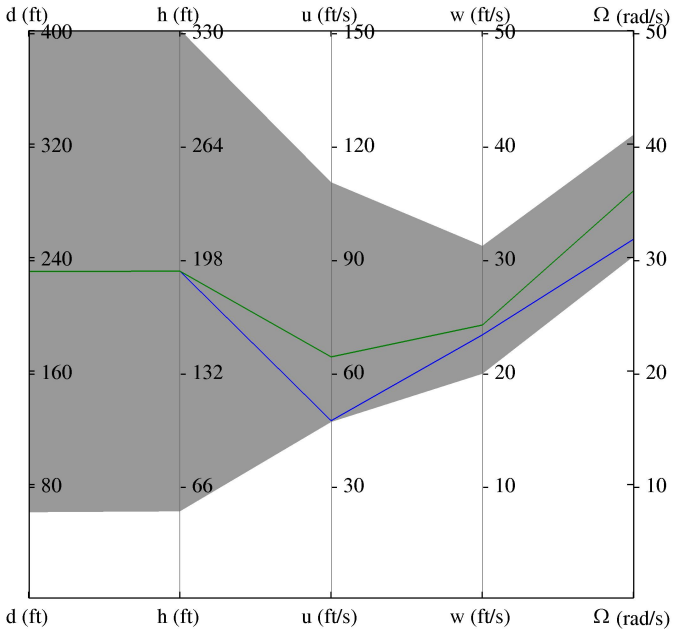

Figure 4.1. Bounded region of the safe landing set for the OH-58 in zero wind.

The safe sets were plotted on the same set of axes in an effort to locate a region of overlap which can be used as a target set of states from which flare should be initiated. This common region would result in the highest likelihood of a safe landing, regardless of wind condition. In all cases the upper limit of the wind range was used (e.g. 10 knots for light wind, 30 knots for moderate wind, and 45 knots for strong wind). The intersection of the safe landing sets for each of these wind conditions (if one exists) indicates the "safest" flare initiation conditions.

4.4 OH-58A Results

4.4.1 OH-58 Vehicle Properties

The Bell OH-58 is a midsize utility helicopter used in both military and civilian applications. It was chosen for analysis due to its similarities to the autonomous Northrop Grumman Fire-X, as well as the availability of its vehicle properties as presented by Lee [17]. The Fire-X offers promising technology for reconnaissance and surveillance missions, and improvement of the vehicle's autorotative capabilities could greatly increase its reliability in the field.

The safe landing set for the OH-58 is generated using candidate initial states seen in Figure 4.2 for the parameters listed in Table 4.1. At the time of initiation, the helicopter is assumed to be in steady state from the descent phase of the trajectory.

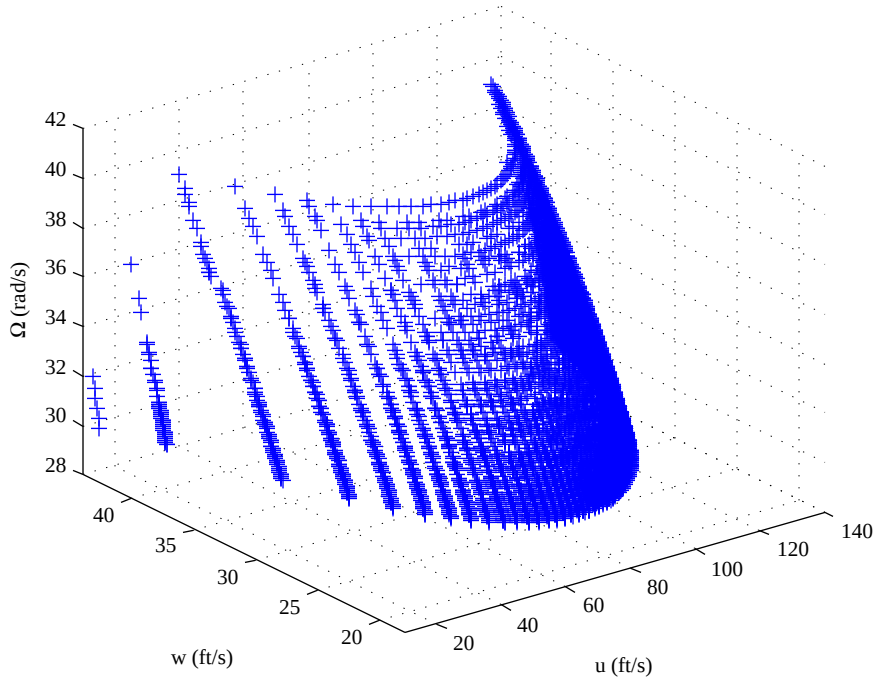

Figure 4.2. Autorotation trim states for the Bell OH-58.

A small portion of the total candidate initial states were tested when generating the safe landing sets. One hundred state combinations were used, which evenly spanned the vehicle's state space, in order to represent the total autorotation state space of the OH-58. The different representative state combinations were tested at each initiation point in the flare region.

The state cost is calculated throughout the trajectory and the touchdown cost is calculated when the helicopter reaches the ground. The state constraints for the OH-58 are shown in Table 4.2 and the safe touchdown conditions are shown in Table 4.3. If a safe, feasible path to touchdown exists, then the initial conditions are a part of the safe landing set.

In Table 4.3, the ground speed limitations for touchdown are given. In truth,

Table 4.1. Parameters of the OH-58A

parameter	symbol	value
blade chord	c	1.33 ft
rotor profile drag coefficient	C_{d0}	0.0087
equivalent flat plate area	f_e	24 ft^2
rotor height	H_R	9.58 ft
main rotor polar moment of inertia	I_R	1344 slug-ft^2
induced power factor	K_{ind}	1.13
number of blades	N_b	2
rotor radius	R	17.63 ft
gross weight	W	3000 lbs
power efficiency factor	η	0.97

Table 4.2. OH-58 State and Control Limits

state/control	symbol	upper	lower
forward airspeed	u	169 ft/s	w_x (ft/s)
descent rate	w	40 ft/s	0 ft/s
rotor speed	Ω	390 RPM	248 RPM
thrust coefficient	C_T	$1.5C_w$	0
tip-path-plane angle	α	$30°$	$-30°$

Table 4.3. OH-58 Touchdown Conditions

state	upper	lower
forward ground speed	+6 ft/s	0 ft/s
descent rate	+8 ft/s	0 ft/s
rotor speed	-	-
horizontal position	+25 ft	-25 ft
time	-	-
aircraft pitch angle	$\theta_{terrain} + 3.65°$	$\theta_{terrain} - 10°$

the helicopter is measuring airspeed, meaning that the touchdown condition on forward speed is equal to the ground speed plus the wind velocity at the center of gravity of the vehicle. Wind will thus still have a significant effect on the helicopter even at touchdown.

4.4.2 OH-58 Safe Landing Sets

The safe landing set for the OH-58 was found for winds ranging from strong headwind through zero wind to strong tailwind. Each landing set was found by defining the wind shear strength and testing various trimmed initial states at different initiation points within the flare region.

Flare is defined as the final stage of autorotation, during which the helicopter is transitioned from a steady-state condition through a series of control inputs in an effort to safely land the helicopter. Initiation is marked by a change in disk orientation and an increase in thrust. This increased thrust is achieved by increasing the collective pitch of the rotor blades. Since no power can be supplied from the engine, this increase in collective will cause a rapid decrease in rotor speed due to the high drag that accompanies higher angles of attack. The limited rotational energy stored in the rotor requires that flare is initiated close to the ground. The flare region therefore represents the region in space (with respect to the landing site) which can realistically be associated with the flare phase of autorotation.

The flare region of tested points for the OH-58 can be seen in Figure 4.3. The horizontal distance ranges from 60 feet to 400 feet from the landing site in increments of 10 feet. The height above the landing site ranges from 50 feet to 330 feet above the landing site in increments of 10 feet. For each wind condition, all candidate autorotation trim states were tested at each point within the flare region.

The upper right region of flare initiation points is dictated by a realistic flight path angle that can be achieved while still landing safely. If the helicopter approaches at too steep of a flight path angle it risks entering the high-altitude-low-velocity region of the height-velocity curve, which generally results in failure during autorotation.

The safe set algorithm was run for the seven wind conditions and the existing safe landing sets were plotted on the same set of axes in an effort to locate a common region of vehicle states under the various wind conditions. This region of overlap can be used as a set of target states to initiate flare which would provide the highest likelihood of a safe landing regardless of wind.

Figure 4.4 shows the five safe landing sets that were found for the various wind

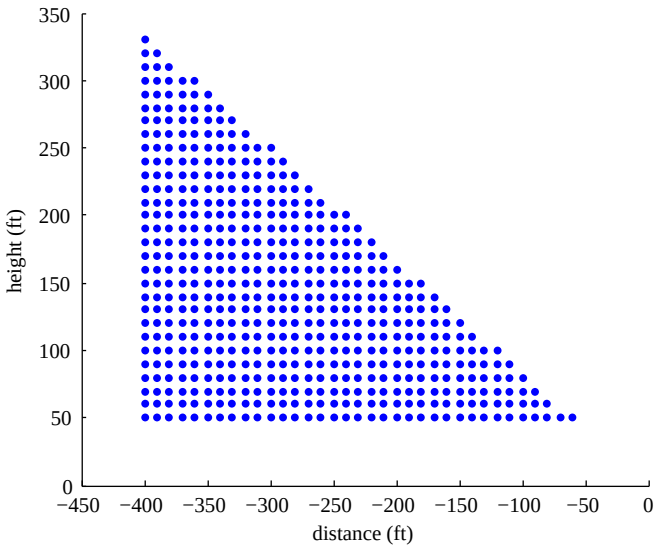

Figure 4.3. Flare region for the OH-58.

conditions. As can be seen, there were no safe landings when the helicopter was acting in moderate or strong tailwinds. This indicates that safe autorotation flare cannot be achieved with greater than light tailwinds. High tailwinds result in a large corresponding ground speed. The helicopter must touchdown in a bounded region that designates a "safe" landing. This requires that the ground speed be reduced to a point that safe touchdown can occur. Since the helicopter is operating under zero power, the high ground speeds associated with strong tailwinds result in either an overshoot of the landing site or excessive ground speeds at touchdown.

Figure 4.4 also shows that there is no common safe region among the remaining five wind conditions. This issue can be approached in two different ways. The first is to never land with a tailwind (even a light tailwind). This will result in an intersecting safe landing set for zero wind to strong headwinds. The second approach is to avoid flaring into a strong headwind, which will leave an intersecting safe landing set for light tailwinds to moderate headwinds. Analyzing the probabilities of occurrence of the possible desired landing conditions would provide guidance to the correct approach. Knowledge of the wind conditions can be utilized by descent phase controllers in order to orient the helicopter into a headwind or tailwind, depending on the wind strength.

Headwinds of increasing magnitude shift the forward airspeed range towards

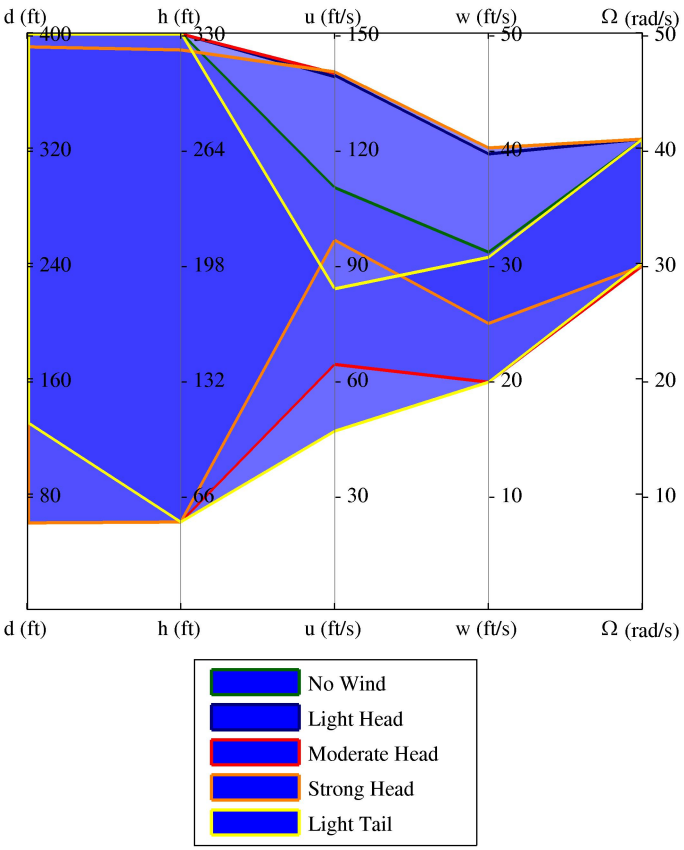

Figure 4.4. Total safe landing set for the OH-58 acting in various wind conditions.

its maximum value, and shifts the initiation point closer to the landing site. This is due to the requirement that the helicopter must always be moving towards the target. The wind velocity, dictated by the shear model, increases with altitude. This velocity places a lower limit on airspeeds which do not violate restrictions. If the wind speed is greater than the airspeed at a given altitude, the helicopter must be moving backwards. This condition would always violate the constraints of the algorithm, causing it to fail. At lower initial altitudes, the wind velocity is also lower, broadening the range of allowable airspeeds.

This is further demonstrated in Fig. 4.5, which shows the flare regions for the OH-58 under the various wind conditions. Each bounded region represents the flare initiation positions that had at least five autorotation trim states that resulted in a safe landing from that point. In the case of flaring into a headwind, increased wind strength shifts the safe flare region closer to the landing site. The low initial

altitudes result in less wind acting on the helicopter, allowing it to land safely.

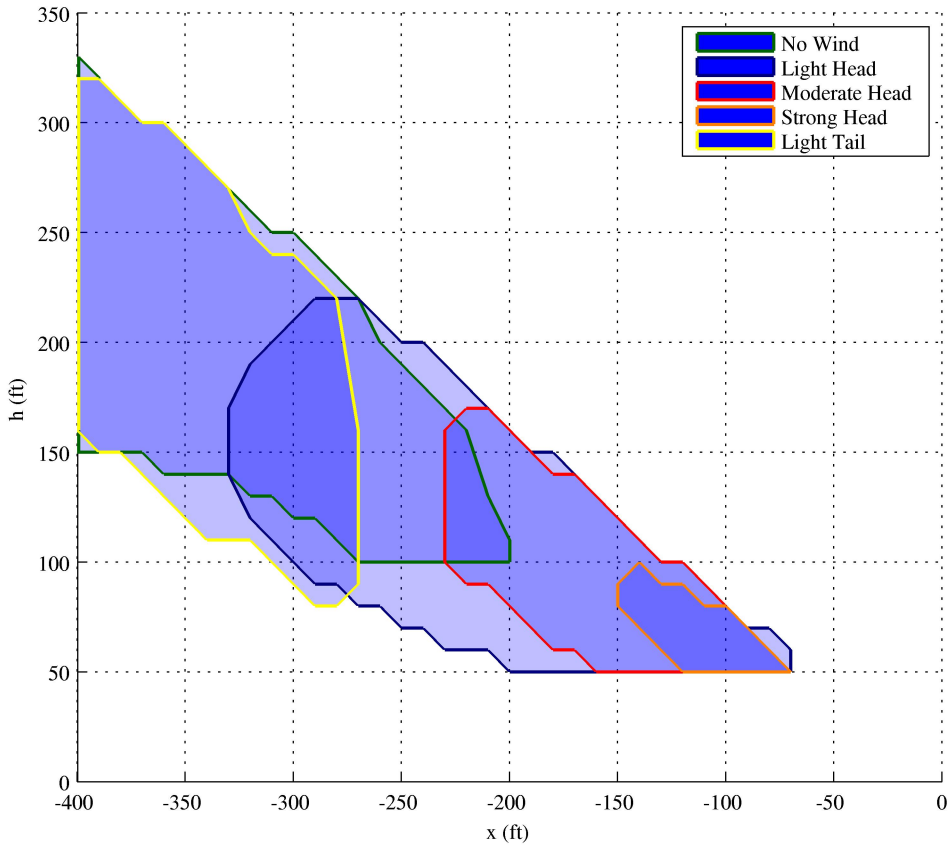

Figure 4.5. Safe flare regions for the OH-58 that result in at least five safe landings for each wind condition.

Flaring through a light headwind generated the widest range of initial states that resulted in a safe landing. This is because the headwind increases the allowable airspeed range at touchdown without being so large that it greatly reduces the state constraints throughout the trajectory. This indicates that for the OH-58, a light headwind (even with wind shear) is beneficial when trying to flare during autorotation.

In order to demonstrate the influence of wind on individual trajectories within the safe landing set, three trajectories were analyzed: one under the influence of a light headwind, one under the influence of a light tailwind, and one flying in zero wind conditions. In each case the flare maneuver was initiated from the same initial states and position. Flare was initiated at a point 340 feet away from, and

240 feet above, the designated touchdown point. The helicopter was flying with a forward airspeed of 49.4 ft/s, a descent rate of 24.2 ft/s, and a rotor speed of 324 RPM, which is 91.5% of the nominal rotor speed.

The ground speeds associated with tailwinds are higher than those associated with headwinds. The result of this can be seen in the Figure 4.6(a), where the trajectory length increases as the wind direction changes from headwind to tailwind. The state history plots in Figure 4.6(b) show the vehicle airspeed, ground speed, descent rate, and rotor speed over the course of the maneuver. As can be seen, flare was initiated from the same set of states (u, w, and Ω) for all three cases. The different wind conditions result in different initial ground speeds and behavior throughout the maneuver. However, in each case the vehicle velocity is decreased to the point where a safe landing can occur within the bounded landing region. The small spike in rotor speed towards the end of the maneuver is due to the fact that the restriction on rotor speed is dropped once the helicopter gets close to the ground and landing is assumed to be imminent.

4.5 Hornet Mini Results

4.5.1 Hornet Mini Vehicle Properties

The Hornet Mini UAV is a small-scale, 55-inch rotor diameter unmanned helicopter designed by Adaptive Flight. It is an autonomous UAV that can be operated in both user-controlled manual mode and autonomous waypoint flight. The Hornet Mini offers a useful platform for testing and implementing flight trajectories in simulation and on real hardware.

The set of steady-state autorotation conditions for the Hornet Mini can be seen in Figure 4.7. A subset of one hundred different state combinations was chosen so that the total range of the state space was represented.

These steady-state conditions were calculated using the vehicle properties seen in Table 4.4. Similar to the OH-58, the safe landing sets were calculated for the Hornet Mini by testing each of the state combinations at the various flare initiation points under different wind conditions.

The Hornet Mini is significantly smaller than the OH-58 and flies at significantly

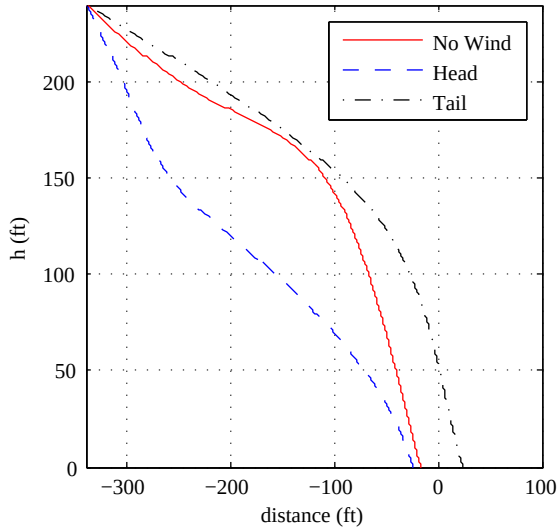

(a) flight path

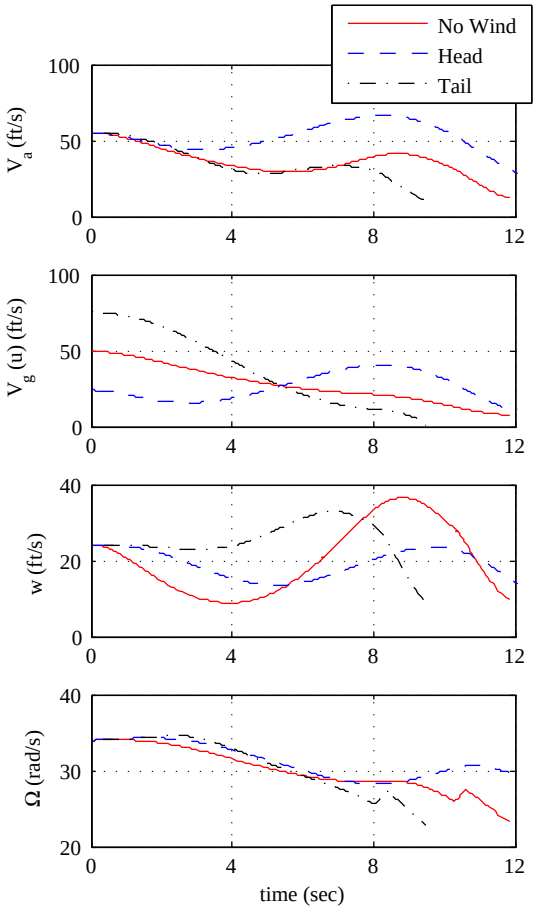

(b) state history

Figure 4.6. Flare trajectories for the OH-58 starting at the same initial conditions under light headwind, light tailwind, and no wind conditions.

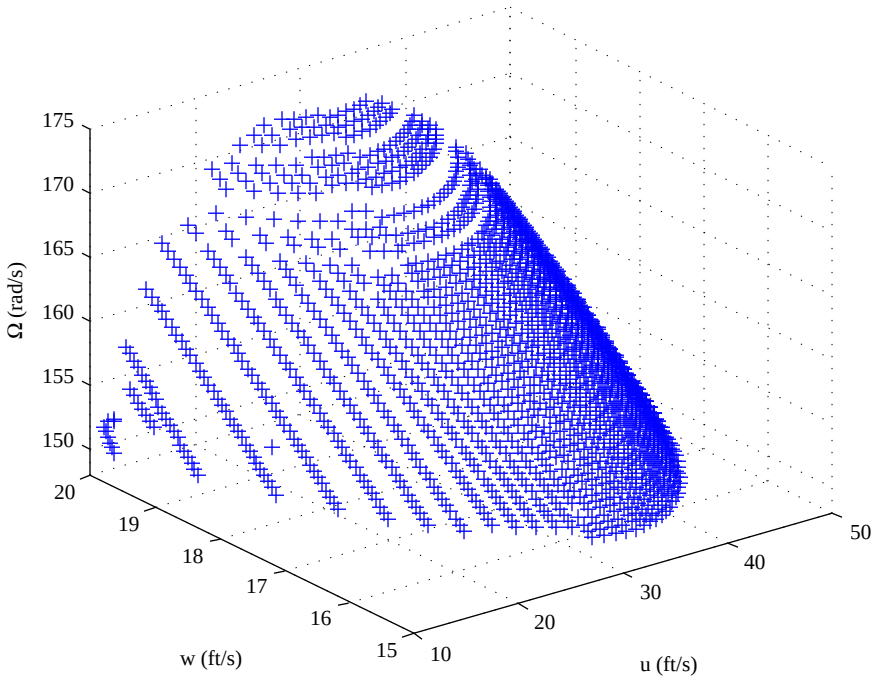

Figure 4.7. Autorotation trim states for Hornet Mini.

Table 4.4. Parameters of the Hornet Mini

parameter	**symbol**	**value**
blade chord	c	0.177 ft
rotor profile drag coefficient	C_{d0}	0.01
equivalent flat plate area	f_e	0.401 ft^2
rotor height	H_R	1.38 ft
main rotor polar moment of inertia	I_R	0.02 slug-ft^2
induced power factor	K_{ind}	1.15
number of blades	N_b	2
rotor radius	R	2.29 ft
gross weight	W	11.6 lbs
power efficiency factor	η	0.9

lower speeds. This is demonstrated by the low airspeed limitations shown in Table 4.5. The safe touchdown conditions for the Hornet can be seen in Table 4.6. Due to the low airspeeds of the vehicle, the bounded landed site is relatively small,

since the helicopter does not need to overcome large ground speeds as compared to the OH-58. However, the high wind shear the vehicle experiences at touchdown can complicate the final moments of the flare maneuver.

Table 4.5. Hornet State and Control Limits

state/control	symbol	upper	lower
forward airspeed	u	50 ft/s	w_x (ft/s)
descent rate	w	20 ft/s	0 ft/s
rotor speed	Ω	1947 RPM	1416 RPM
thrust coefficient	C_T	$1.5C_w$	0
tip-path-plane angle	α	$30°$	$-30°$

Table 4.6. Hornet Touchdown Conditions

state	upper	lower
forward ground speed	+5 ft/s	0 ft/s
descent rate	+6 ft/s	0 ft/s
rotor speed	-	-
horizontal position	+10 ft	-10 ft
time	-	-
aircraft pitch angle	$\theta_{terrain} + 5°$	$\theta_{terrain} - 5°$

4.5.2 Hornet Mini Safe Landing Sets

A similar process was used to find the safe landing sets for the Hornet Mini UAV. The Hornet is considerably smaller and slower than the OH-58, which results in a correspondingly smaller flare region, which can be seen in Figure 4.8. The horizontal distance of the region ranges from 15 feet to 50 feet from the landing site in five foot increments. The height above the landing site ranges from 10 feet to 30 feet, also in five foot increments. In addition to the lower airspeeds, the Hornet also has less rotational inertia in the rotor, meaning there is less available energy to arrest a high descent rate. This contributes to the limited size of the flare region. Different vehicle state combinations are tested at each point in the

flare region, and those trim states that result in a safe landing are members of the safe landing set.

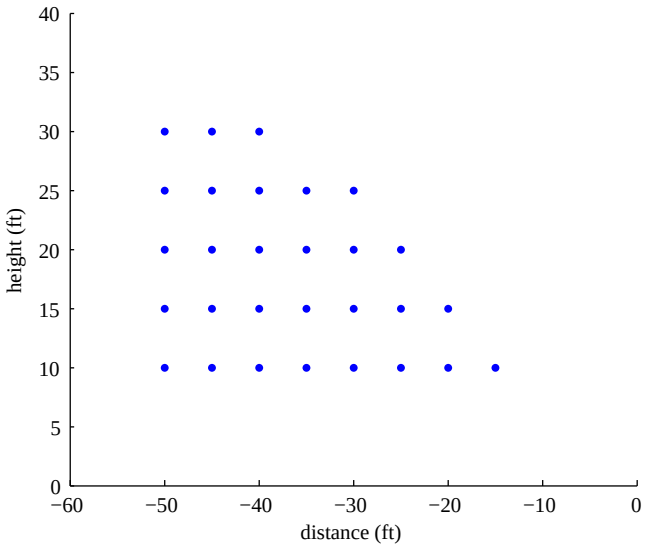

Figure 4.8. Flare region for the Hornet Mini.

The small size of the Hornet Mini means that it is strongly influenced by the high wind shear it experiences at touchdown. The logarithmic wind model of Equation (2.7) has a very high gradient close to the ground. This high shear complicates the final moments of touchdown, as the helicopter experiences rapid changes in wind velocity which limits the size of the safe landing set.

The safe landing sets for the Hornet Mini can be seen in Figure 4.9. There were no safe landings when operating in a severe headwind. This is because the wind speeds associated with this profile strength are higher than the Hornet's maximum airspeed, even at low altitudes. This means that the helicopter would have to be moving backwards, which violates the constraints of the algorithm.

There were also no conditions where safe flare could occur in tailwinds. Due to the small size and the limited stored energy of the Hornet Mini, the high ground speeds associated with tailwinds make landing impossible. Under these conditions, the Hornet Mini either overshoots the landing site, or is unable to reduce its ground speed to within the safe bounds during touchdown.

As can be seen in Figure 4.9 the ideal flare initial states live near their respective maximum values. Conversely, the initiation points are close, both vertically and

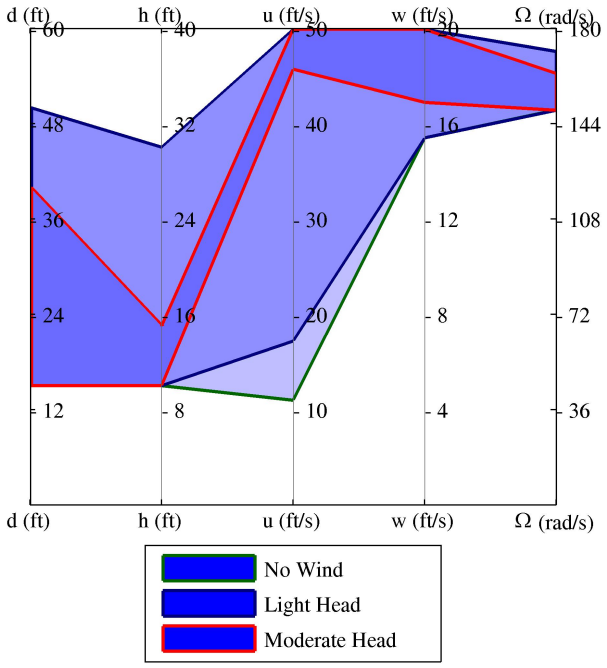

Figure 4.9. Total safe landing set for the Hornet Mini acting in various wind conditions.

horizontally, to the landing site. High wind conditions greatly constrict the flare region that results in safe landings. When operating in a moderate wind condition, the Hornet must fly fast and flare late. As opposed to the OH-58, calmer conditions are ideal in order to maximize the flare success rate of the Hornet.

To show the influence of wind on the flight of the Hornet, a flare trajectory was generated for the same set of initial states under light headwind and no wind conditions (the tailwind condition was omitted because none exist). The trajectories can be seen in Figure 4.10(a) and the state comparisons can be seen in Figure 4.10(b). Initiation occurred 50 feet away from and 20 feet above the desired touchdown point. The path was generated using an initial forward speed of 38.5 ft/s, descent rate of 19.5 ft/s, and rotor speed of 1600 RPM, which was 90.4% of the nominal rotor speed for this helicopter.

4.6 H-V Diagram

The height-velocity (H-V) diagram is a standard means of visualizing the flight conditions under which successful autorotation can be achieved. For single en-

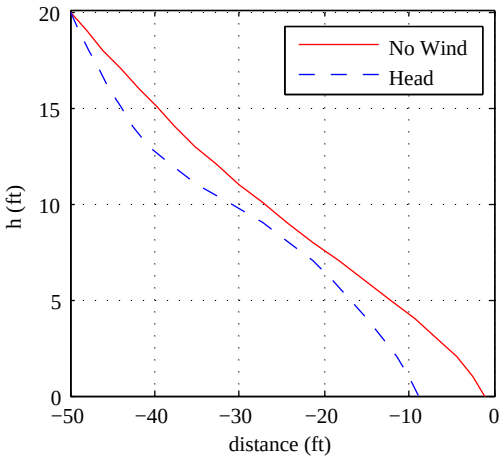

(a) flight path

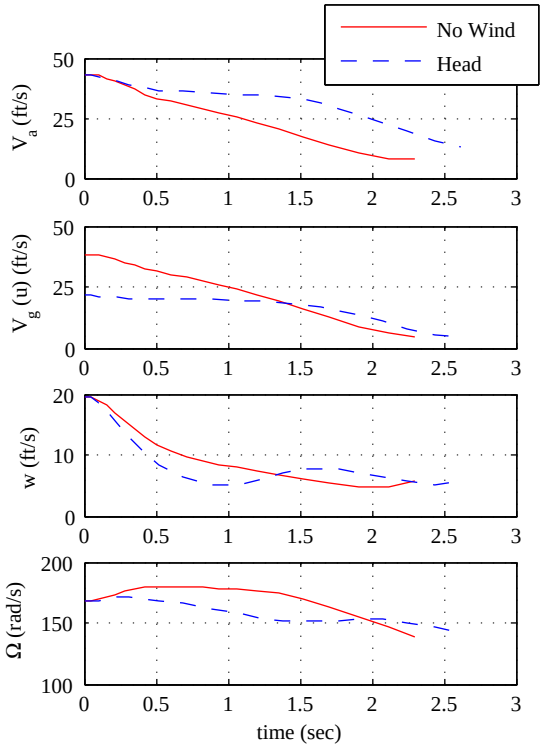

(b) state history

Figure 4.10. Flare trajectories for the Hornet Mini starting at the same initial conditions under light headwind and no wind conditions.

gine helicopters there are generally two regions of the H-V curve which should be avoided when entering autorotation (called the deadman's curve). The H-V diagram for the OH-58 can be seen in Figure 4.11 [18]. The avoid region at low altitudes and high airspeeds defines the flight conditions under which failure would occur due to pilot reaction time. If engine failure occurs in this region, the aircraft would lose altitude and crash before the pilot could safely begin autorotating. The second, larger avoid region represents high altitude - low velocity flight conditions. In this region, the helicopter is too high to survive a vertical landing and is flying at too low of an airspeed to avoid the vortex ring state during descent. Additionally, the vehicle cannot gain enough forward airspeed required to enter a steady glide.

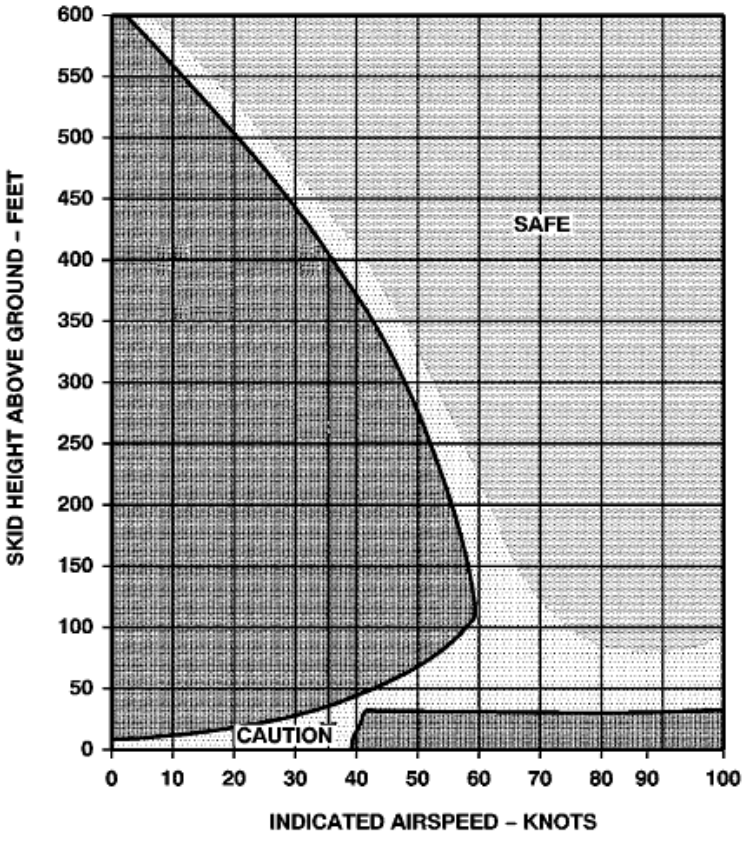

Figure 4.11. H-V diagram for the OH-58 [18].

It would stand to reason that a projection of the safe landing set onto the H-V diagram would allow for a comparison of the two safe set visuals. However, there are several differences which result in discrepancies between the safe sets. First,

the H-V diagram assumes that the helicopter will enter and proceed through the entire autorotation maneuver, whereas the safe landing set only accounts for the final flare phase of autorotation. The H-V diagram also assumes that the helicopter is in straight and level flight during which a power loss may occur. This allows for a wider range of velocities to be taken into account. Since the safe landing set only accounts for flare, the velocity range is limited to steady-state descent conditions [2]. Finally, if engine failure occurs at high velocity and low altitude (just above the high-speed, no-fly area), the aircraft can balloon up, trading airspeed for altitude, and then enter into autorotation. The flare problem assumes that the vehicle is always descending, and thus altitude gain is impossible.

These discrepancies can be seen by comparing Figure 4.11 with Figure 4.12, which shows the H-V diagram generated from the safe landing set of the OH-58 acting in zero wind. A majority of the safe landings occur at low airspeeds. This is due mainly to the fact that the safe set algorithm must account for the location of the landing site. Since the helicopter must touchdown at a designated location, the vehicle position and velocity at initiation are crucial to the success of the maneuver. Flare that is initiated with high airspeeds generally result in unsafe landings because the helicopter overshoots the landing site. Low airspeeds enable the vehicle to arrest its forward airspeed and descent rate to within allowable limits while also achieving touchdown within the bounds of the landing site.

For the reasons listed, the standard H-V diagram cannot be compared to the H-V diagram generated from the safe landing set. The simulated H-V diagram does offer some information about possible safe landings, however there are more efficient means of visualizing the safe landing set.

4.7 Summary

This chapter presents the results of the safe landing set algorithm for the OH-58 and the Hornet Mini under a range of wind conditions.

Section 4.1 briefly reviews the methodology for computing the safe landing set. A subset of steady-state autorotation conditions is tested at each initiation point in the flare region. The trajectory is optimized by minimizing a cost function dependent on vehicle states and controls. Any combinations that result in a safe

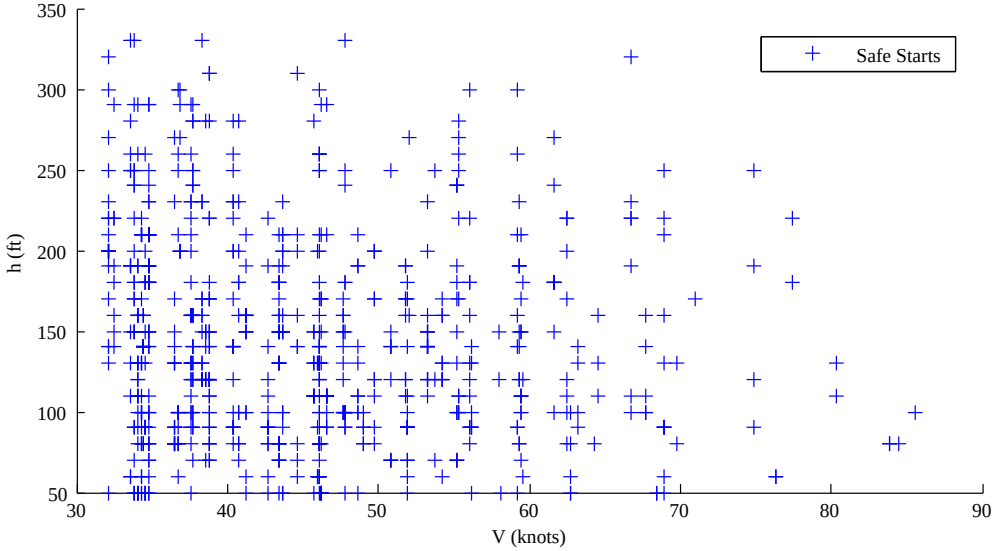

Figure 4.12. H-V diagram for the OH-58 from the safe landing set.

landing are members of the safe landing set. This process is repeated for conditions ranging from strong tailwinds to strong headwinds.

Section 4.2 outlines the visualization technique used in this thesis in order to represent the safe landing set. This is done using parallel coordinates, in which each state occupies its own coordinate along the x-axis. All state combinations that result in a safe landing are scaled and plotted in order to effectively visualize the safe landing set.

Next, the results of the wind shear analysis is presented. For each helicopter, the algorithm was run for light, moderate, and severe headwinds and tailwinds, as well as a zero wind condition, in an effort to locate a common set of safe states. This region can be used as a set of target states to initiate flare that will result in the highest likelihood of a safe landing, regardless of wind conditions.

Section 4.4 presents the results for the OH-58. In Section 4.4.1, the properties of the OH-58 are discussed. The OH-58 is a midsize utility helicopter that was chosen due to its similarities to the autonomous Northrop Grumman Fire-X, as well as the availability of its vehicle properties from previous studies.

Section 4.4.2 presents the safe landing sets that were found for the OH-58 acting in various wind conditions. It was discovered that safe flare cannot be achieved while operating in a tailwind greater than light strength. Additionally,

there was no common region among the five remaining safe sets. This problem can be approached in one of two ways: never land with a tailwind, or avoid flaring into a strong headwind. It was also discovered that flaring into a light headwind results in the widest range of initial states from which safe flare can be initiated.

Section 4.5 presents the results for the Hornet Mini. Vehicle properties are presented in Section 4.5.1. The Hornet Mini is a small-scale autonomous helicopter designed by Adaptive Flight. It is much smaller and slower than the OH-58, and the flare region is correspondingly smaller.

The safe landing sets for the Hornet are presented in Section 4.5.2. No safe landings occurred when operating in a severe headwind because the wind speed was greater than the vehicle's maximum airspeed. Additionally, there were no safe landings when operating in a tailwind of any strength. The high ground speeds associated with tailwinds resulted in either an overshoot of the landing site or ground speeds that exceeded acceptable limitations upon touchdown.

The small size of the Hornet Mini causes it to be highly influenced by wind shear near touchdown. For this reason, the vehicle must fly fast and flare late when operating in a headwind. The widest range of safe states was found when operating in zero wind.

In Section 4.6, the H-V diagram from the OH-58 operator's manual is presented and compared to the H-V diagram from the safe landing set. This is generally the standard means of evaluating safe operational conditions for helicopters. However, since the safe landing set only investigates the flare phase of autorotation, the two H-V diagrams cannot be effectively compared.

Chapter 5

Flight Simulation Results

5.1 Description of Vehicle

The Hornet Mini UAV is a small-scale, 55-inch rotor diameter unmanned helicopter designed by Adaptive Flight, Inc [19]. It is an autonomous vehicle that can be operated in both user-controlled manual mode and autonomous waypoint flight. The helicopter's onboard avionics utilize GPS, inertial sensors, a magnetometer, and an air pressure measurement in order to navigate and provide inner loop flight control [20]. A data link relays the vehicle's states to the ground control station, allowing the operator to provide commands to the helicopter.

Waypoint control can be used to generate and carry out flight trajectories by placing waypoints at desired locations. Each waypoint contains a GPS location, an altitude, and a velocity, and the onboard avionics generates a flight trajectory between these points such that the required end conditions are met. Waypoint flight was used to implement flare trajectories in simulation.

5.2 Waypoint-Generated Flare Trajectory

As a means of validating the flare trajectories generated by the safe set algorithm, a maneuver was tested in the simulation environment using waypoint control (this also served to ensure that a safe landing was achievable for future hardware tests). The trajectory was created using three waypoints. The first "initiation" waypoint

was placed in the center of the safe landing set to ensure that the proper initial conditions were achieved. The second "stop at" waypoint was placed at the touchdown location with zero commanded velocity in order to achieve a safe landing. The final waypoint was an "entry" waypoint placed some distance away from the initiation waypoint in order to achieve the proper descent angle and velocity for initiation. The onboard controller generated a trajectory between these waypoints that met the desired endpoint criteria. In practice, the touchdown waypoint was placed a small distance above the ground (about three feet) to account for overshoot. The trajectory can be seen in Figure 5.1.

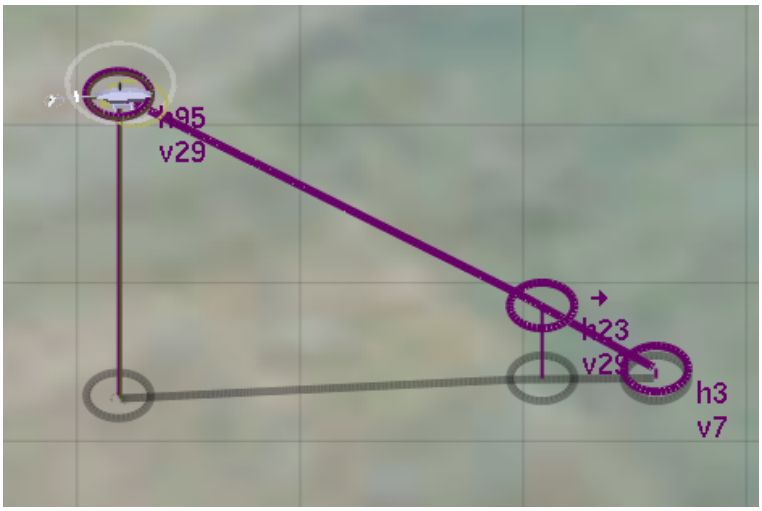

Figure 5.1. Hornet simulation flare trajectory using three waypoints for entry, initiation, and touchdown.

A flare initiation condition near the middle of the Hornet's zero-wind safe landing set (Figure 4.9) was defined as a waypoint: $x = 30$ feet, $h = 20$ feet, $u = 23.1$ ft/s, $w = 18.6$ ft/s, and $\Omega = 1562$ RPM. Placing the touchdown waypoint at an altitude of three feet resulted in a safe landing, with planned and actual touchdown conditions given in Table 5.1. Note that touchdown at a vertical speed of 3 ft/s is equivalent (in terms of energy) to the helicopter being dropped to the ground from a height of two inches.

A comparison of planned and simulated trajectories is shown in Figure 5.2. The top plot shows the planned and simulated flight paths, as well as the vehicle location and pitch orientation at 0.2 second intervals (note: the images are not to scale). As can be seen, the flight paths are very similar. The simulator attempts

Table 5.1. Hornet Mini planned and simulated touchdown conditions (using GPS waypoint navigation).

state	planned	simulated
u	4.3 ft/s	3.1 ft/s
w	5.5 ft/s	3.1 ft/s

to land the helicopter at the desired waypoint, which in this case represents the origin, while the safe set algorithm attempts to land the helicopter within 10 feet of the origin. As a result, the touchdown points differ slightly. Similarly, the simulator attempts to reduce the vehicle velocity to as close to zero as possible upon landing, whereas the algorithm only attempts to decrease the velocity to a point that safe touchdown can occur.

Forward speed, descent rate, and rotor speed vary more smoothly in the GPS-waypoint simulated trajectory. This can be attributed partially to the higher order dynamics modeled in the simulator (recall that the trajectory generator used in the safe set computation is a point-mass model). Additionally, waypoint control only allows for the command of vehicle states at certain points throughout the maneuver. The safe set algorithm controls the vehicle at each step along the trajectory, and the fluctuations in control inputs cause variations in vehicle states on the way to touchdown.

The control inputs (longitudinal cyclic and collective pitch) were plotted as a fraction of maximum possible value. The bottom two plots of Figure 5.2 show that both controls are well within bounds, indicating that the flare trajectory is not "over-taxing" the vehicle's control authority.

5.2.1 Waypoint Height Sensitivity

In order to ensure that GPS waypoint control is an effective means of generating a flare trajectory, the robustness of the system was investigated. This was done by testing the sensitivity of safe touchdown to the height of the touchdown waypoint above ground and the position of the flare initation waypoint. The aim of this investigation was to ensure that a crash landing would not occur if there were minor discrepancies between the true vehicle position and the commanded

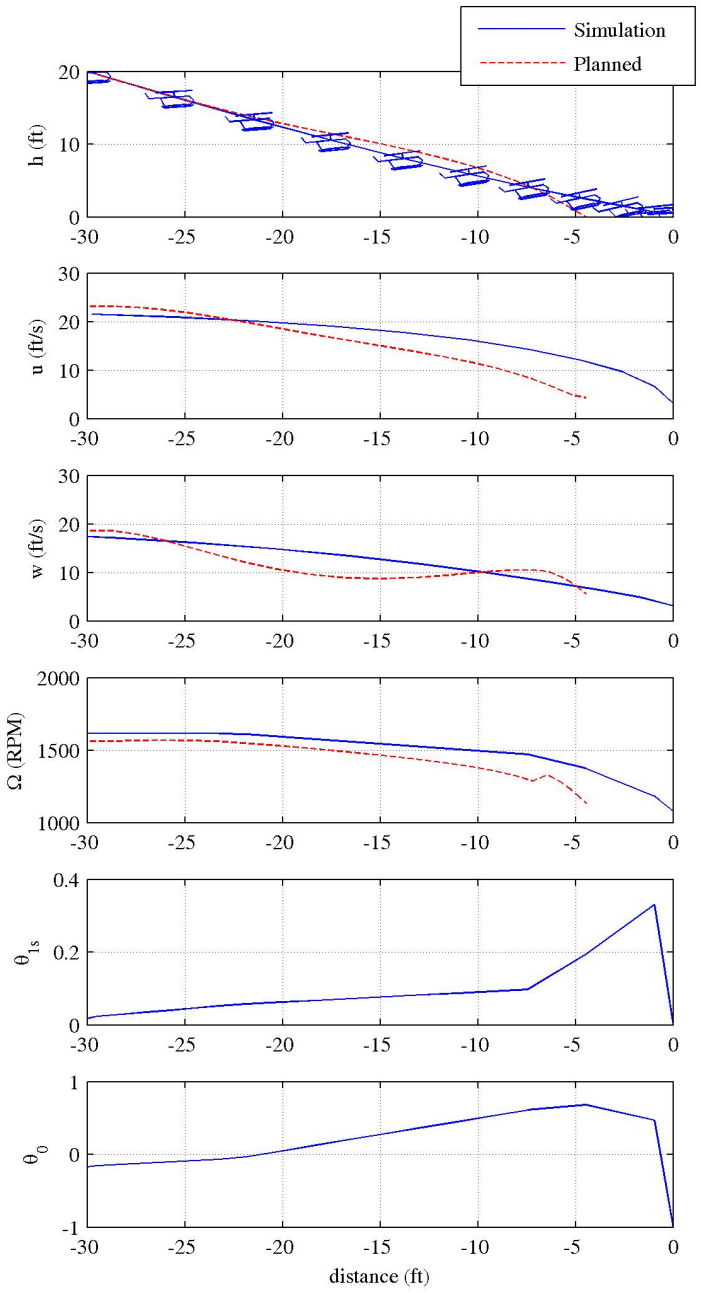

Figure 5.2. Comparison of the planned Hornet flare maneuver with the simulated maneuver. (Note: the helicopter images are not drawn to scale).

vehicle position. The flare initiation waypoint height was varied ±2 feet around the nominal value of 20 feet and the touchdown waypoint height was varied from one foot above ground to four feet above ground. The resulting flare trajectories can be seen in Figure 5.3.

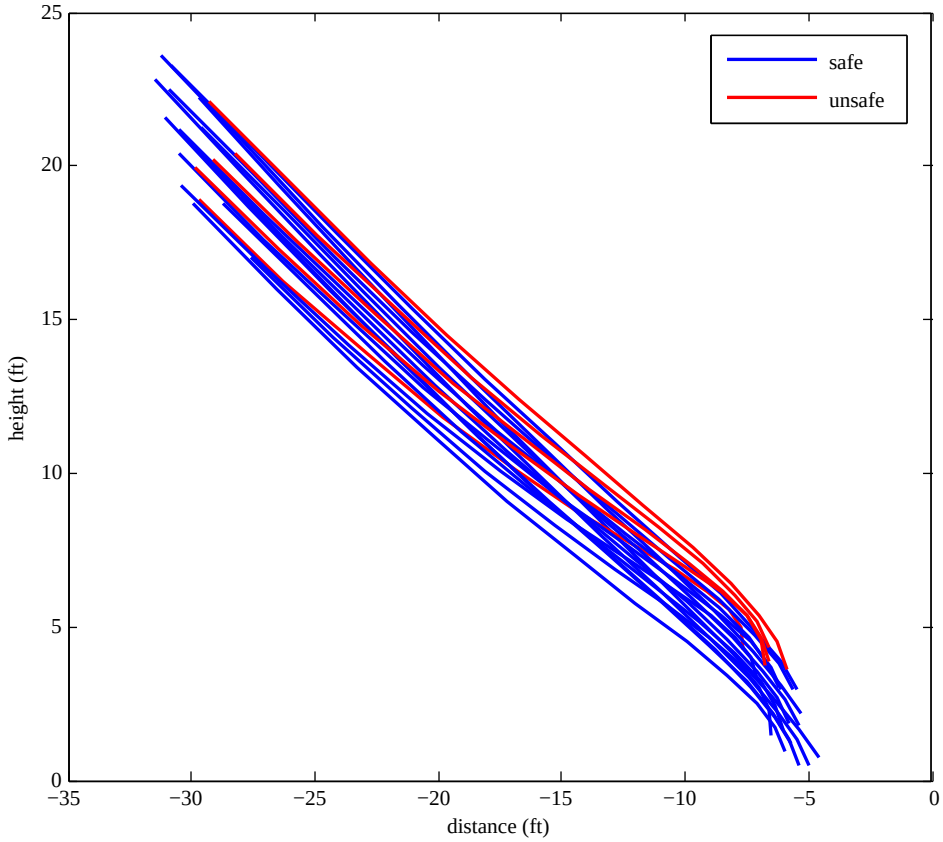

Figure 5.3. Multiple flare trajectories for various initiation and touchdown waypoint height combinations.

Safe flare cannot be achieved when the touchdown waypoint is above three feet. At this height, the loss of rotor speed that accompanies an increase in collective pitch occurs while the vehicle is still relatively high above the ground. This causes the helicopter to fall from the sky, and the touchdown descent rate to exceed safe bounds.

Figure 5.3 also shows that successful landings are much more dependent on touchdown waypoint height than on initiation waypoint height. For a particular touchdown waypoint (below four feet), the helicopter was able to land safely,

regardless of initiation height. This is because the small variation in initiation altitude has little effect on the glide path of the vehicle during flare.

This investigation gives confidence in the use of GPS waypoint control for flare trajectories, and means that the ultimate purpose of the safe set algorithm (which was to generate the set of safe flare initial conditions) is broadly applicable to rotorcraft autorotation.

5.3 Summary

This chapter presents results of individual flare maneuvers executed in the Hornet Mini simulation environment.

Section 5.1 gives a brief description of the Hornet Mini UAV. The Hornet is a small-scale, 55-inch rotor diameter unmanned helicopter that can be operated in both user-controlled manual mode and autonomous waypoint flight. The helicopter uses various sensors in order to navigate, and relays flight data to the operator.

Section 5.2 presents simulation results of a flare maneuver executed on the Hornet Mini. GPS waypoint control was used to generate the trajectory: the first "initiation" waypoint lives in the center of the safe landing set; the second "touchdown" waypoint is a zero-velocity waypoint that allows safe landing to occur; the third "entry" waypoint is placed some distance away from the initiation waypoint in order to achieve the proper descent path and velocity for initiation.

A comparison of the planned and simulated trajectories shows similar results. There were minor discrepancies in vehicle states between the two cases, due mainly to the higher order dynamics that are modeled in the simulator. However, in each case the helicopter was able to touchdown within acceptable bounds, demonstrating that GPS waypoint control is a viable means of executing flare trajectories on the Hornet Mini.

In Section 5.2.1 the sensitivity of safe landings to the altitude of the initiation and touchdown waypoints was investigated. Safe landings cannot occur if the touchdown waypoint is higher than three feet off the ground. From this height, the rotor stalls while the helicopter is still in the air, and a crash landing occurs. The altitude of the initiation waypoint does not have a significant effect on the success of the maneuver.

Chapter 6

Conclusion

Small, autonomous helicopters represent a highly effective technology in the area of surveillance and reconnaissance missions. Their ability to hover and operate in tight quarters offer advantages over their fixed-wing UAV counterparts. However, their wide-scale use in the field is dependent on the reliability and recoverability of the vehicle in the event of engine failure. In single engine helicopters (which represent most UAV helicopters) power failure is known to be recoverable through autorotation.

Autorotation is the flight condition the helicopter enters when it loses power to its main rotor. It is defined by four main phases: engine failure, entry, steady-state descent, and flare. Upon engine failure the pilot (or autopilot) must decrease the collective in order to maintain rotor RPM. During descent, the air flowing up through the rotor keeps it spinning, and a safe landing site is identified. Once the vehicle is sufficiently close to the ground, flare is initiated. This is marked by a change in rotor plane orientation and an increase in collective in an effort to arrest vehicle velocity so that safe touchdown can occur.

Flare is the final and most difficult stage of autorotation. It occurs very quickly and very close to the ground, and limited rotational kinetic energy is available to slow the vehicle's descent. Timing is crucial to the success of the maneuver, as an increase in collective causes a large buildup of drag which results in decreased thrust. If flare is initiated too early, rotor speed is bled off and the helicopter falls out of the sky. If flare is initiated too late, the helicopter cannot decrease its velocity to within acceptable limits, and a crash landing occurs. The correct

flare initiation location is highly dependent on the vehicle state during the descent phase of autorotation.

There have been previous studies into autonomous autorotation, and while these studies have yielded promising results, they all assume ideal conditions. In reality, wind and wind shear have a large influence on the trajectory of the helicopter, particularly during flare. As the vehicle descends through shear, the wind velocity decreases, causing a change in airspeed. Due to the limited energy available to arrest the descent rate, the wind severity plays a significant role in the success of the flare maneuver.

6.1 Summary of Contributions

6.1.1 Effect of Wind Shear on the Safe Landing Set

The primary focus of this thesis was to investigate the influence of wind and wind shear on the safe landing set: the set of all steady-state autorotation conditions, combined with initiation points, from which a safe path to touchdown is guaranteed to exist. In order to effectively model wind shear, a two-dimensional logarithmic shear profile was used. It is accurate for relatively low altitudes, which makes it suitable for flare analysis. Its mathematical representation enables it to be added to existing equations of motion in order to model airspeed. Additionally, it can be explicitly modeled as either a headwind or a tailwind of varying magnitudes. Throughout the analysis three different shear profile strengths were investigated: light, moderate, and severe. The safe landing sets were generated for each wind condition in an effort to identify a set of steady-state conditions that is shared among the various sets. This region can be used as a target set of states from which flare should be initiated which will result in the highest probability of a safe landing, regardless of wind conditions.

6.1.2 Safe Landing Sets for the OH-58 and Hornet Mini Flying Through Wind Shear

The safe landing sets were generated for two helicopters: the Bell OH-58 and the Adaptive Flight Hornet Mini. For each helicopter, the safe set algorithm was run for light, moderate, and severe headwinds and tailwinds, as well as a zero wind case. The OH-58 was chosen for analysis due to the availability of its vehicle properties from previous studies, as well as its similarities to the Northrop-Grumman Fire-X autonomous helicopter. The Hornet Mini is a small-scale, 55-inch rotor diameter, unmanned helicopter designed by Adaptive Flight, Inc. This vehicle was used to validate the safe set algorithm using the helicopter's simulation environment.

It was shown that wind has a significant effect on the flare trajectory of a helicopter. For the OH-58, safe flare cannot be achieved when operating in a tailwind greater than light strength. The high associated ground speeds resulted in either an overshoot of the landing site or touchdown velocities that exceeded acceptable bounds. Additionally, there was no common safe region among the remaining five wind conditions. This problem can be approached by: a) never landing with a tailwind, or b) avoiding flaring into a strong headwind. Knowledge of the wind conditions can be used by a descent phase controller in order to orient the vehicle during approach. It was also discovered that, for the OH-58, flaring into a light headwind is beneficial, as it generates the widest range of steady-state conditions that result in a safe landing.

The Hornet Mini is much smaller and flies much slower than the OH-58, and the safe landing sets for the Hornet support this fact. No safe landings were found when operating in a tailwind of any strength. Tailwinds cause high ground speeds, and since there is limited energy available to arrest the descent, the vehicle either overshoots the landing site or has velocities that exceed limitations upon touchdown. There were also no safe landings when operating in a severe headwind, as the wind speed was greater than the Hornet's maximum airspeed. The widest range of safe states was found when operating in zero wind. This is because the small size of the Hornet makes it highly susceptible to wind shear close to the ground. By comparing the results for the OH-58 with the results of the Hornet Mini, it can be seen that vehicle size is an important factor when analyzing the

influence of wind shear on autorotation flare. Small, lightweight helicopters are much more susceptible to the effects of wind and wind shear.

6.1.3 Simulation Results

The Hornet Mini simulation environment was used to test and validate flare trajectories. The trajectory was generating using three waypoints: the first "initiation" waypoint lives in the middle of the safe landing set; the second "touchdown" waypoint is a zero-velocity waypoint located at the landing site in order to achieve a safe landing; the final "entry" waypoint is placed some distance away from the initiation waypoint in order to achieve the proper descent path and velocity for initiation.

A comparison of the planned and simulated trajectories showed similar flight paths. Forward speed, descent rate, and rotor speed showed small discrepancies between the planned and simulated cases, due mainly to the higher order dynamics modeled in the simulator. However, the touchdown conditions for both cases fell within the bounds that constitute a safe landing, meaning GPS waypoint control is an acceptable means of implementing flare trajectories on the Hornet Mini.

6.2 Recommendations for Future Work

6.2.1 Landing Site Selection

The safe landing set is a backwards reachable set, meaning that the location of the landing site must be known in order for the algorithm to work. The vehicle's initial states, which constitute the safe landing set, are determined relative to the landing site. If the true touchdown location differs from the estimated touchdown location, the safe set algorithm is ineffective.

Since the flare initiation conditions correspond to the vehicle state at the end of the steady-state descent, the whole of the autorotation maneuver is dependent on the touchdown location. In reality, the helicopter may be flying over cluttered ground when engine failure occurs, and the identification of an acceptable landing site would happen in real time during the descent phase of autorotation.

6.2.2 Robustness of Safe Set Algorithm

Currently, the safe set algorithm assumes that the wind conditions are known prior to initiation, and those conditions remain constant throughout the descent. However, in real flight, a poor estimate of, or a change in, wind speed can occur, which would cause a change in the true airspeed and flare path during the maneuver. It may be beneficial to test various trajectories from one landing set under the influence of various other wind conditions, and compare the flight paths and state histories in order to validate the robustness of the safe set algorithm.

6.2.3 Hardware Implementation Using Waypoint Control

The work done in the Hornet simulator has demonstrated that GPS waypoint control is a viable means of implementing flare trajectories on the Hornet Mini. Future work includes a hardware demonstration of a full flare maneuver using the Hornet Mini UAV. Before flying the helicopter, GPS position data should be collected and analyzed in order to ensure that the vehicle's position measurement will not drift over the course of the flight, as an accurate reading of altitude is crucial to the success of the maneuver. After performing the flare maneuver, flight data can be retrieved and compared to the simulated case as well as the planned case.

6.2.4 Full Trajectory Implementation on the Hornet Mini

The flare trajectory implemented in the Hornet Mini simulator utilizes waypoint following control. The vehicle velocity and position are explicitly defined at three points along the path, and the Hornet's onboard avionics generates a flight trajectory such that the required end conditions are met. Though a successful autorotation is achievable, there are discrepancies between the planned and simulated trajectories in simulation. In the future, a fully generated trajectory can be implemented on the Hornet Mini using Adaptive Flight's external guidance software.

Bibliography

[1] Leishman, J. G. (2006) *Principles of Helicopter Aerodynamics*, chap. 5, Cambridge University Press, New York, NY.

[2] Tierney, S. and J. W. Langelaan (2010) "Autorotation Path Planning using Backwards Reachable Sets and Optimal Control," in *Proceedings of the 66th AHS Annual Forum*, Phoenix, Arizona.

[3] Yomchinda, T., J. F. Horn, and J. W. Langelaan (2012) "Autonomous Control and Path Planning for Autorotation of Unmanned Helicopter," in *American Helicopter Society 68th Annual Forum*, Fort Worth, TX.

[4] ——— (2011) "Flight Path Planning for Descent Phase Helicopter Autorotation," in *AIAA Guidance, Navigation and Control Conference*, Portland, OR.

[5] Johnson, W. (1977) "Helicopter Optimal Descent and Landing after Power Loss," in *Technical Memorandum TM 73244*, NASA Ames Research Center.

[6] Floros, M. W. (2009) "DESCENT Analysis for Rotorcraft Survivability with Power Loss," in *American Helicopter Society 65th Annual Forum*.

[7] Bachelder, E. N. and B. L. Aponso (2003) "Using Optimal Control for Helicopter Autorotation Training," in *Proceedings of the American Helicopter Society 59th Annual Forum*, Phoenix, AZ.

[8] Carlson, E. B. (1999) *Optimal Tiltrotor Aircraft Operations During Power Failure*, Ph.D. thesis, University of Minnesota, Minneapolis, MN.

[9] Abbeel, P., A. Coates, T. Hunter, and A. Y. Ng (2008) "Autonomous Autorotation of an RC Helicopter," in *International Symposium on Robotics*.

[10] Aponso, B., D. Lee, and E. N. Bachelder (2005) "Evaluation of a Rotorcraft Autorotation Training Display on a Commercial Flight Training Device," in *Proceedings of the American Helicopter Society 61st Annual Forum*, Grapevine, Texas.

[11] Atkins, E. M., I. A. Portillo, and M. J. Strube (2006) "Emergency Flight Planning Applied to Total Loss of Thrust," *Journal of Aircraft*, **43**(4), pp. 1205–1216.

[12] Holsten, J., S. Loechelt, and W. Alles (2010) "Autonomous Autorotation Flights of Helicopter UAVs to Known Landing Sites," in *American Helicopter Society 66th Annual Forum*, Phoenix, AZ.

[13] Sprinkle, J., J. M. Eklund, and S. S. Sastry (2005) "Deciding to Land a UAV Safely in Real Time," in *Americna Controls Conference*.

[14] Bayen, A. M., I. M. Mitchell, M. M. K. Oishi, and C. J. Tomlin (2007) "Aircraft Autolander Safety analysis Through Optimal Control-Based Reach Set Computation," *Journal of Guidance and Control*, **30**(1), pp. 68–77.

[15] (1997) *MIL-STD-1797A: Flying Qualities of Piloted Aircraft*, *Tech. rep.*, Department of Defense, Washington DC.

[16] Aponso, B. L., E. N. Bachelder, and D. Lee (2005) "Automated Autorotation for Unmanned Rotorcraft Recovery," in *American Helicopter Society International Specialist Meeting on Unmanned Rotorcraft*, Chandler, AZ.

[17] Lee, A. Y., A. E. B. Jr., and W. S. Hindson (1988) "Optimal Landing of a Helicopter in Autorotation," *Journal of Guidance, Control, and Dynamics*, **11**(1), pp. 7–12.

[18] Department of the Army, Washington, D.C. (2010) *Operator's Manual Army Model OH-58 A/C Helicopter*, 17 ed.

[19] Adaptive Flight, Inc. (2012) *Operating Handbook Hornet Mini UAS*, version 10216-1 ed.
URL `www.adaptiveflight.com`

[20] Yomchinda, T., N. Grande, J. F. Horn, and J. W. Langelaan (2013) "Development and Testing of an Autonomous Autorotation System," in *AHS Unmanned Rotorcraft and Network Centric Operations Specialists' Meeting*, Scottsdale, AZ.